Gondwana Research 128 (2024) 106–126

Contents lists available at ScienceDirect

Gondwana Research

journal homepage: www.elsevier.com/locate/gr

Early Paleozoic extensional tectonics along Gondwana's northern margin: Insights from Iran

Yousef Zoleikhaei [a,*], Jacob A. Mulder [a,b], Peter A. Cawood [a]

[a] School of Earth, Atmosphere and Environment, Monash University, Melbourne, Victoria 3800, Australia
[b] Department of Earth Sciences, University of Adelaide, Adelaide, South Australia 5005, Australia

ARTICLE INFO

Article history:
Received 7 July 2023
Revised 17 October 2023
Accepted 17 October 2023
Available online 14 November 2023
Handling Editor: I. Safonova

Keywords:
Gondwana
Ordovician
Iran
Detrital zircon
Detrital rutile

ABSTRACT

The Paleozoic tectonic evolution of the northern margin of Gondwana is inferred to comprise several episodes of continental breakup and ocean opening. However, the timing and number of rifting events, and the identity and paleogeography of the continental blocks involved in these inferred breakup events remain poorly understood. This study examines the early Paleozoic tectonic evolution of northern Gondwana by analyzing the paleogeography and provenance of Ordovician strata exposed in the Iranian blocks. New detrital zircon U–Pb–Hf measurements from Ordovician siliciclastic strata in Iran define two major age fractions at 600—500 Ma (41 %; $\varepsilon Hf_{(t)}$ = −11.9 to +9.6) and 1100—600 Ma (37 %; $\varepsilon Hf_{(t)}$ = −21.6 to +10.6), and two minor fractions at > 1100 Ma (13 %; $\varepsilon Hf_{(t)}$ = −13.9 to +5.9) and 500—444 Ma (10 %; $\varepsilon Hf_{(t)}$ = −9.1 to +4.4). Detrital rutile U–Pb ages from these units similarly include two major age fractions at 1100—600 Ma (49 %) and 600—500 Ma (33 %), and two minor fractions at > 1100 Ma (14 %) and 500—444 Ma (4 %). Zr-in-rutile temperatures and Cr–Nb compositions indicate that most detrital rutiles are sourced from amphibolite facies metapelitic or metafelsic rocks. The new data suggest sediment was ultimately sourced from the Arabian-Nubian Shield (~54 %) and 600—500 Ma (~39 %) and Ordovician (~7%) magmatic rocks in local basement in Iran. The widespread exposure of 600—500 Ma magmatic rocks in Iran indicates significant changes in basin configuration from a stable platform in the Ediacaran—Cambrian to a series of fault-bound extensional basins in the Ordovician. We explore two possible scenarios for the Ordovician extension in Iran. The first involves detachment of a continental block from northern Iran leading to opening of the Paleo-Tethys Ocean. However, because the identity of this hypothesized rifted continental block remains unclear, we interpret that early to middle Paleozoic extension across the region occurred within an already established continental margin.

1. Introduction

Continental blocks derived from northern Gondwana make up most of modern Eurasia, and are delineated by belts of ophiolites, magmatic arc rocks, and collisional orogens (Stöcklin, 1974; Shafaii Moghadam and Stern, 2014; Moghadam and Stern, 2015; Torsvik and Cocks, 2017; Wu et al., 2020; Metcalfe, 2021; Robertson et al., 2021). The Ediacaran to late Cenozoic assembly of this collage of continental blocks is interpreted to have involved the intermittent formation and consumption of Tethyan ocean basins through the detachment and northward migration of continental blocks from northern margin of Gondwana (NMG; Fig. 1A) (Stampfli et al., 1991; Stampfli and Borel, 2002; Metcalfe, 2021). Continental breakup associated with each phase of rifting was not simultaneous along the margin and there is no consensus on the number and timing of continental breakup episodes, nor the original location of the detached blocks (Torsvik and Cocks, 2017; Wu et al., 2020; Metcalfe, 2021; Robertson et al., 2021).

The history of episodic continental rifting and the transfer of continental fragments to Eurasia via closure of Tethyan ocean basins is best known from the geological record of Eurasia with comparatively fewer constraints from the northern Gondwana margin (e.g., Shafaii Moghadam and Stern, 2014; Moghadam and Stern, 2015; Metcalfe, 2021). The poorly-resolved opening stages of these oceanic basins has hindered their spatial and temporal correlations along the NMG and understanding the tectonic drivers

* Corresponding author.
E-mail addresses: yousef.zoleikhaei@monash.edu, yousef.zoleikhaei@yahoo.com (Y. Zoleikhaei).

https://doi.org/10.1016/j.gr.2023.10.017
1342-937X/

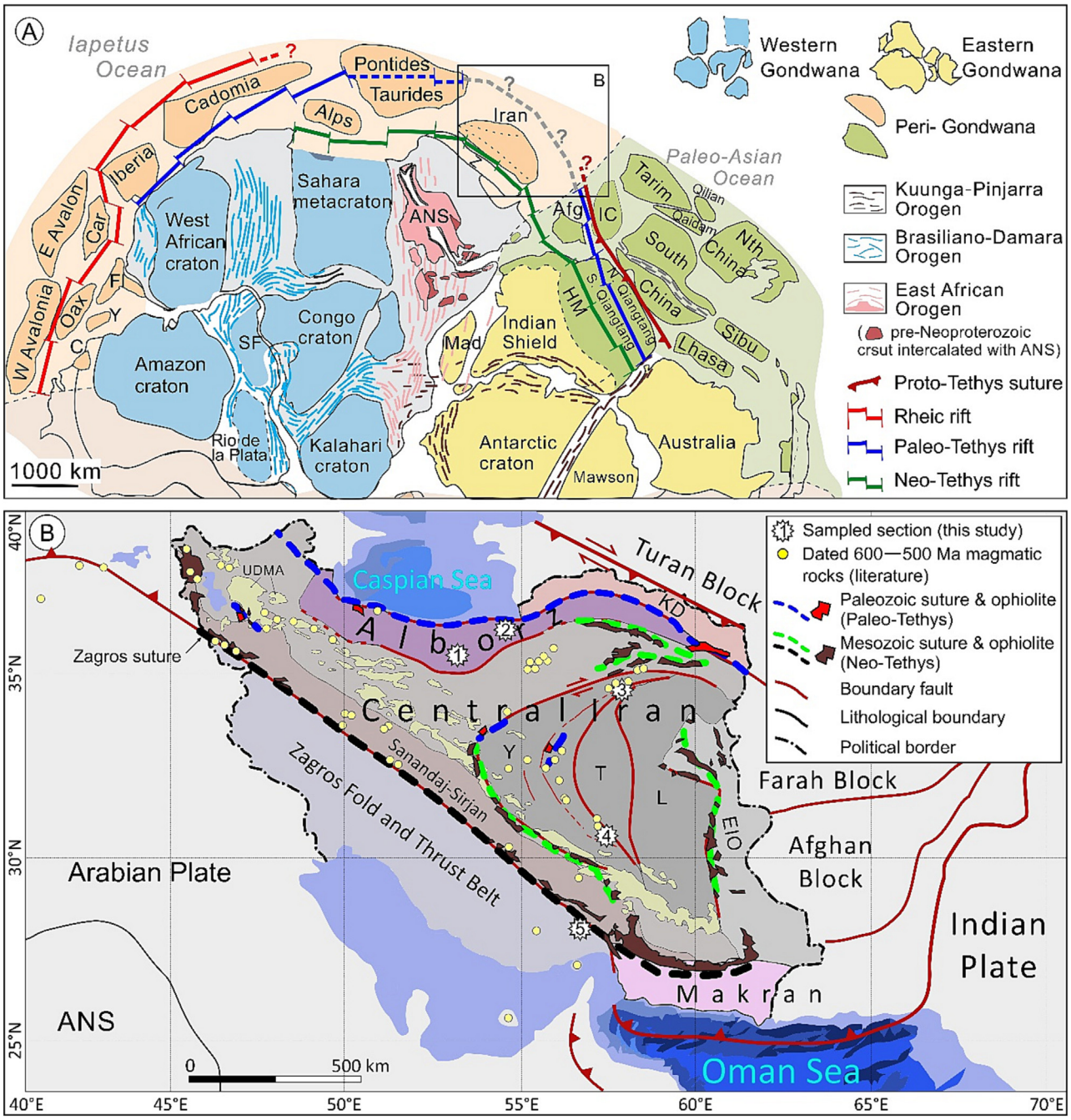

Fig. 1. A) Paleogeographic map of Gondwana (modified from Cawood et al., 2021) showing core continental blocks, *peri*-Gondwanan blocks, major interior orogens, and inferred locations of continental breakup and ocean basin formation. Note that unlike other segments of the NMG, no fringing block to the north of Iran has been identified that could have rifted away during the inferred opening of the Paleo-Tethys Ocean. Openings of the Paleo- and Neo-Tethys oceans along the NMG were diachronous. B) Geological map of Iran showing main structural blocks, bounding faults, ophiolitic sutures, and studied sections. Note that Paleo-Tethys-related ophiolites are found in several locations inboard (southwest) from the main inferred paleo-Tethys suture zone in NE Iran (i.e., the dashed blue line). Black suture belt is related to the Neo-Tethys Ocean closure, and the green suture belts are related to closure of back-arc extensional basins associated with Neo-Tethys subduction. Y: Yazd block, T: Tabas block, L: Lut block, UDMA: Urumieh-Dokhtar Magmatic Arc, KD: Kope Dagh; EIO: East Iranian Orocline. (For interpretation of the references to colour in this figure legend, the reader is referred to the web version of this article.)

and paleogeographic implications of this rift history (Torsvik and Cocks, 2017). These ambiguities are most pronounced for the older Ediacaran to middle Paleozoic continental breakup events, mainly because a detailed reconstruction of the NMG during this period is lacking, and the rock record of these older events, now in central Eurasia, is heavily overprinted by younger orogenic events.

In this paper, we outline an early Paleozoic paleogeographic reconstruction of the northern margin of Gondwana (NMG) abutting the Sahara Metacraton and the Arabian Plate and present new geochronological data to refine models for the early Paleozoic tectonothermal evolution of this region. Our goal is to better understand the paleogeography and tectonic context of early Paleozoic extension along the northern margin of Gondwana and their relationship to the formation of the Paleo-Tethys Ocean. For this purpose, we employ a multi-proxy provenance analysis of Ordovician siliciclastic successions from the NMG fringing the Arabian

Plate, including detrital zircon U–Pb and Hf isotope and detrital rutile U–Pb and trace element analyses. This integrated dataset provides insight into the age and genesis of magmatism and the metamorphic history of the source region, which helps to refine models for the Ordovician tectonomagmatic evolution of the NMG. We focus on the Ordovician siliciclastic successions in the Alborz, Central Iran, and Zagros blocks of Iran. These blocks are located to the south of the Paleo-Tethys suture, which now lies in Eurasia, and are considered to have formed the southern flank of the Paleo-Tethys rift along the NMG (e.g., Stampfli et al., 1991; Stampfli and Borel, 2002; Álvaro et al., 2022). Importantly, these Iranian blocks preserve a nearly continuous history of Ediacaran to Ordovician sedimentation, offering an extensive record of early Paleozoic extension along the NMG. We combine the new data with geological constraints from Eurasia (i.e., the Paleo-Tethys suture) to revise paleogeographic and tectonic models for the early Paleozoic transfer of continental blocks between Gondwanan and Eurasia.

2. Geological setting

Iran consists of three main structural blocks, Alborz, Central Iran, and Zagros, which are differentiated based on their deformation style, bounding faults, and fringing ophiolites (Fig. 1B) (Stöcklin, 1968, 1974; Berberian and King, 1981). From the Ediacaran to late Paleozoic, the Iranian blocks formed part of the Arabian Plate along the NMG (Becker et al., 1973; Soffel and Rster, 1980; Wensink, 1983; Vecoli and Le Hérissé, 2004; Ghavidel-syooki and Vecoli, 2008; Spina et al., 2020a). Following the late Paleozoic opening of the Neo-Tethys Ocean along the Zagros suture, the Alborz and Central Iran blocks rifted away from Gondwana as part of the Cimmerian terranes (e.g., Central Iran, Alborz, Taurides, Afghanistan, South Qiangtang; Fergusson et al., 2016; Hassanzadeh and Wernicke, 2016; Sheikholeslami, 2017; Jamei et al., 2020; Jamei et al., 2021). The northward migration of the Cimmerian terranes and their collision with the southern margin of Eurasia involved subduction and closure of the Paleo-Tethys Ocean in Permian-Triassic (Fig. 1) (Wilmsen et al., 2009; Zanchi et al., 2009a; Rahmati-Ilkhchi et al., 2010; Kargaranbafghi et al., 2012; Zanchetta et al., 2013; Zanchi et al., 2015; Zanchi et al., 2016). Following, and probably concurrent with Paleo-Tethys closure, northward movement of the Afro-Arabian Plate initiated subduction of the Neo-Tethys oceanic crust under Central Iran. This subduction is recorded by arc magmatism in the western-southwestern margins of Central Iran (i.e., the Urmia-Dokhtar magmatic arc), metamorphism in the Sanandaj-Sirjan zone, and widespread extensional back-arc basins in Central Iran and Alborz blocks, which locally developed into narrow seaways floored by oceanic crust (Fig. 1B) (Monsef et al., 2014; Monsef et al., 2018a; Monsef et al., 2018b; Moghadam et al., 2019; Shafaii Moghadam et al., 2020b; Monsef et al., 2022). The final collision of the Arabian plate with Central Iran, probably in the Eocene-Miocene, formed the Zagros Fold and Thrust Belt as part of the transcontinental Alpine-Himalaya Orogen (e.g., Stöcklin, 1968; Berberian and King, 1981; Agard et al., 2011; Barber et al., 2018; Gholami Zadeh et al., 2020; Gholami Zadeh et al., 2021; Koshnaw et al., 2021). This compressional tectonism inverted the Neo-Tethyan back-arc extensional basins in Central Iran and Alborz blocks, where obducted ophiolites represent the remnants of these narrow oceans are exposed farther north of the Neo-Tethys suture, and in some cases are in close spatial association with the Paleo-Tethyan ophiolites in NE Iran (Fig. 1B) (Khalatbari Jafari et al., 2013; Moghadam and Stern, 2015; Moghadam et al., 2019; Pirnia et al., 2020).

The oldest crystalline rocks in the Iranian blocks include bimodal (mafic—felsic) plutonic and rare volcanic rocks ranging in age from 600 Ma to 500 Ma (Fig. 1B) (e.g., Hassanzadeh et al., 2008; Rossetti et al., 2015; Moghadam et al., 2016; Moghadam et al., 2017b; Shafaii Moghadam et al., 2017; Honarmand et al., 2018; Daneshvar et al., 2019; Gholipour et al., 2022; Moradi et al., 2022; Nouri et al., 2022). Based on whole-rock geochemistry, contrasting tectonic models have been suggested for the origin of these magmatic rocks including a continental magmatic arc (e.g., Ramezani and Tucker, 2003; Shafaii Moghadam et al., 2020a; Moghadam et al., 2021) or an extensional back-arc zone (e.g., Sepidbar et al., 2020; Sepidbar et al., 2021; Azizi and Whattam, 2022).

Ediacaran—Cambrian sedimentary successions in Iran include mixed siliciclastic and carbonate sequences plus minor volcanic intercalations with the distribution of lithofacies indicating a change from isolated fault-bound basins in the Ediacaran to a unified shallow marine sedimentary basin during the Cambrian (Fig. 2) (Berberian and King, 1981; Geyer et al., 2014; Bayet-Goll et al., 2015; Bayet-Goll et al., 2018; Ghorbani, 2019). The laterally extensive lithofacies, absence of angular unconformities, and consistent provenance form the Arabian-Nubian Shield (ANS) have been interpreted to indicate that the Cambrian strata were deposited in a north/northeast-facing, epicontinental basin that lacked significant local topography (Horton et al., 2008; Zoleikhaei et al., 2021, 2022).

Ordovician magmatic rocks in Iran include mostly thin (<50 m) mafic volcanic interlayers within sedimentary strata, which locally form thicker units (~ 700 m) in some sections; for example, the Soltan Meydan Basalts in eastern part of the Alborz block (Bagheri and Stampfli, 2008; Derakhshi and Ghasemi, 2015; Derakhshi et al., 2017; Fatehi and Ahmadipour, 2018; Vesali et al., 2020; Derakhshi et al., 2022), and minor plutonic rocks (Ghavidel-Syooki et al., 2011b; Moghadam et al., 2017a; Ranjbar Moghadam et al., 2018; Shirdashtzadeh et al., 2018). The Ordovician basalt and gabbro rocks have alkaline to sub-alkaline geochemical affinities, and the rare granitic rocks are A-type granites, and are interpreted to imply extensional tectonics for Iran during this period (Mehdizadeh Shahri, 2008; Derakhshi et al., 2017; Moghadam et al., 2017a; Ranjbar Moghadam et al., 2018; Vesali et al., 2020; Derakhshi et al., 2022). Ordovician sedimentary units in Iran include thick successions of sandstones, shales, and minor conglomerates, which record a marked lithological change from the unconformably underlying carbonate rocks of the middle to late Cambrian Mila Formation (Fig. 2). The Ordovician units are not ubiquitous and, in some sections, younger units, up to Permian age, directly overlie Cambrian strata (Ghavidel-syooki, 1994b; Ghorbani, 2019; Spina et al., 2020b; Bayet-Goll et al., 2022b). The Ordovician siliciclastic successions are compositionally immature and characterized by rapid lateral changes in lithofacies (Bayet-Goll et al., 2022b). They include the Lashkarak and Ghelli formations in the Alborz block (Bayet-Goll and Carvalho, 2017; Álvaro et al., 2022; Bayet-Goll et al., 2022a; Bayet-Goll et al., 2022b), the Shirgesht Formation in the Central Iran block (Bayet-Goll et al., 2016; Khazaei et al., 2018; Bayet-Goll, 2022), and the Zardkuh and Seyahou formations in the Zagros block (Fig. 2) (Asghari, 2014; Vennin et al., 2015). The Ordovician age of these units is mostly based on their fossil content and stratigraphic position (Ghavidel-syooki, 1994a, 2006; Ghobadi Pour et al., 2006; Schallreuter et al., 2006; Ghobadi Pour and Popov, 2009; Evans et al., 2013; Ghavidel-Syooki et al., 2014; Ghobadi Pour et al., 2015; Kebria-ee Zadeh et al., 2015; Popov et al., 2015; Ebbestad et al., 2016; Ghavidel- Syooki, 2019; Ghobadi Pour, 2019; Ghavidel-Syooki, 2021). Paleocurrent data are highly variable and indicate north, east, and southward sediment transport directions

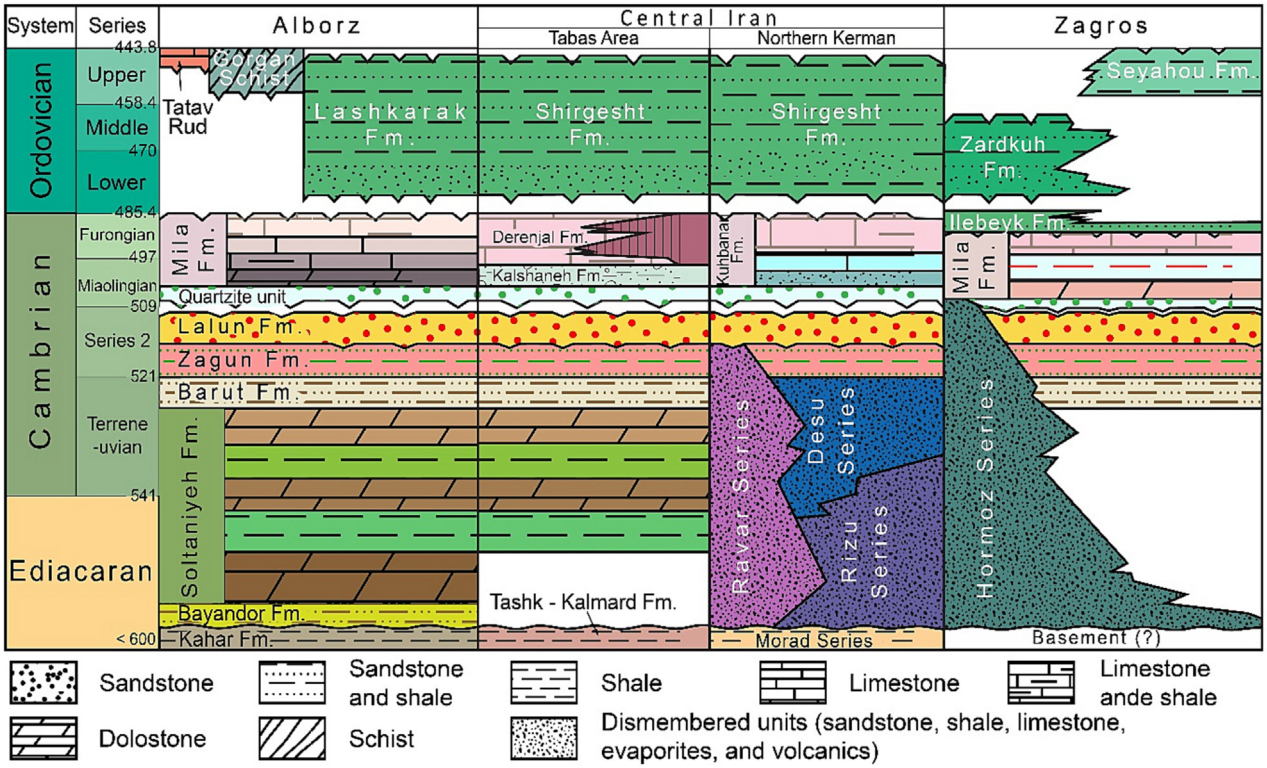

Fig. 2. Simplified Ediacaran—Ordovician stratigraphic column of Iran (modified from Aghanabati and Rezaei, 2009) showing correlative sedimentary units across the Alborz, Central Iran, and Zagros blocks.

(Bayet-Goll et al., 2016; Bayet-Goll and Neto de Carvalho, 2016; Bayet-Goll et al., 2022b).

Large-scale paleovalleys with grooved and striated boulders in the infilling late Ordovician sediments in the eastern and northern margins of the Arabian Shield are interpreted to preserve evidence for (super)continental-scale glaciation during the late Ordovician (Clark-Lowes, 2005; Masri, 2017). Similarly, Ghavidel-syooki et al. (2011a) believe that the upper parts of the Ordovician successions in the Zagros block include glaciomarine detritus, which mark the northern/northeastern extents of the late Ordovician ice sheet.

3. Methods

We collected samples from the laterally extensive Ordovician sedimentary units in the three blocks of Iran including the Lashkarak, Shirgesht, Zardkuh, and Seyahou formations (Fig. 2). Fig. 3 shows the stratigraphic column of the Ordovician units in the studied sections, geographic coordinates and stratigraphic locations of the samples, number of samples per unit, and type of detrital mineral analyses. A variety of names have been applied to the Ordovician stratigraphic units in the Dehmolla section of the Alborz block. Here, we use the name Lashkarak Formation for the whole Ordovician interval, which includes the Lashkarak and Ghelli formations of Ghavidel-syooki (2006), and the unnamed unit and Lashkarak Formation of Ghobadi Pour (2019), and the ~70 m thick interval of submature sandstone below these strata (Fig. 3).

Our analyses include detrital zircon U–Pb analyses on 11 samples (a total of 979 grains), and detrital zircon Lu–Hf (283 grains) and detrital rutile U–Pb and trace element (368 grains) analyses on 4 representative samples (Fig. 3). Sample preparation and analysis were carried out at the Isotopia Facility, Monash University. Detrital grains were hand-picked from heavy mineral fractions separated using heavy liquids and magnetic separation and mounted into epoxy resin blocks. The mounts were then polished to expose the middle of the grains. Cathodoluminescence (CL) images for zircon grains and back scattered electron (BSE) images for the rutile grains were used to select analytical spots. Detrital zircon U–Pb analyses were conducted via LA-ICP-MS following the method outlined in Matthews and Guest (2017), which involved 15 s ablation with a laser beam of 25 μm spot size, 4 j.cm^{-2} on-sample fluence, and a repetition rate of 8 Hz. A subset of detrital zircons were also analyzed for Lu–Hf isotopes via LA-MC-ICP-MS following the method detailed in Mulder et al. (2021). Both Lu–Hf and U–Pb isotopic data were collected for these grains via split-stream analyses, which involved 60 s of ablation using a laser beam with a 35 μm spot size, 4.5 j.cm^{-2} on-sample fluence, and a repetition rate of 8 Hz. Most U–Pb and Lu–Hf measurements were collected from the same CL domains of the grains analyzed during the first U–Pb session. However, some new grains were also analyzed as some of the grains analyzed for U–Pb isotopes in the first session were too small to place a second laser spot for U–Pb–Hf measurements. Detrital rutile U–Pb and trace element (^{27}Al, ^{45}Sc, ^{47}Ti, ^{51}V, ^{52}Cr, ^{55}Mn, ^{56}Fe, ^{57}Fe, ^{59}Co, ^{89}Y, ^{90}Zr, ^{93}Nb, ^{95}Mo, ^{118}Sn, ^{178}Hf, ^{181}Ta, ^{182}W, ^{206}Pb, ^{208}Pb, ^{232}Th, ^{238}U) analyses were conducted via split stream LA-ICP-MS, in which the grains were ablated for 30 s using a laser beam with 35 μm spot size, 6.5 j.cm^{-2} on-sample fluence, and 10 Hz repetition rate. All data were reduced using the *Iolite 4* software package (Paton et al., 2011). Data tables for zircon U–Pb and Lu–Hf, rutile U–Pb and trace element, and reference materials analyses used for calibrating the experiments and assessing data accuracy are provided in supplementary files A, B, C, and D. The detrital zircon and rutile U–Pb ages include both concordant (< ±10 % discordant; discordance = (^{207}Pb/^{235}U ÷ ^{206}Pb/^{238}U − 1) × 100) and discordant (> ±10 discordant) data. Given that no

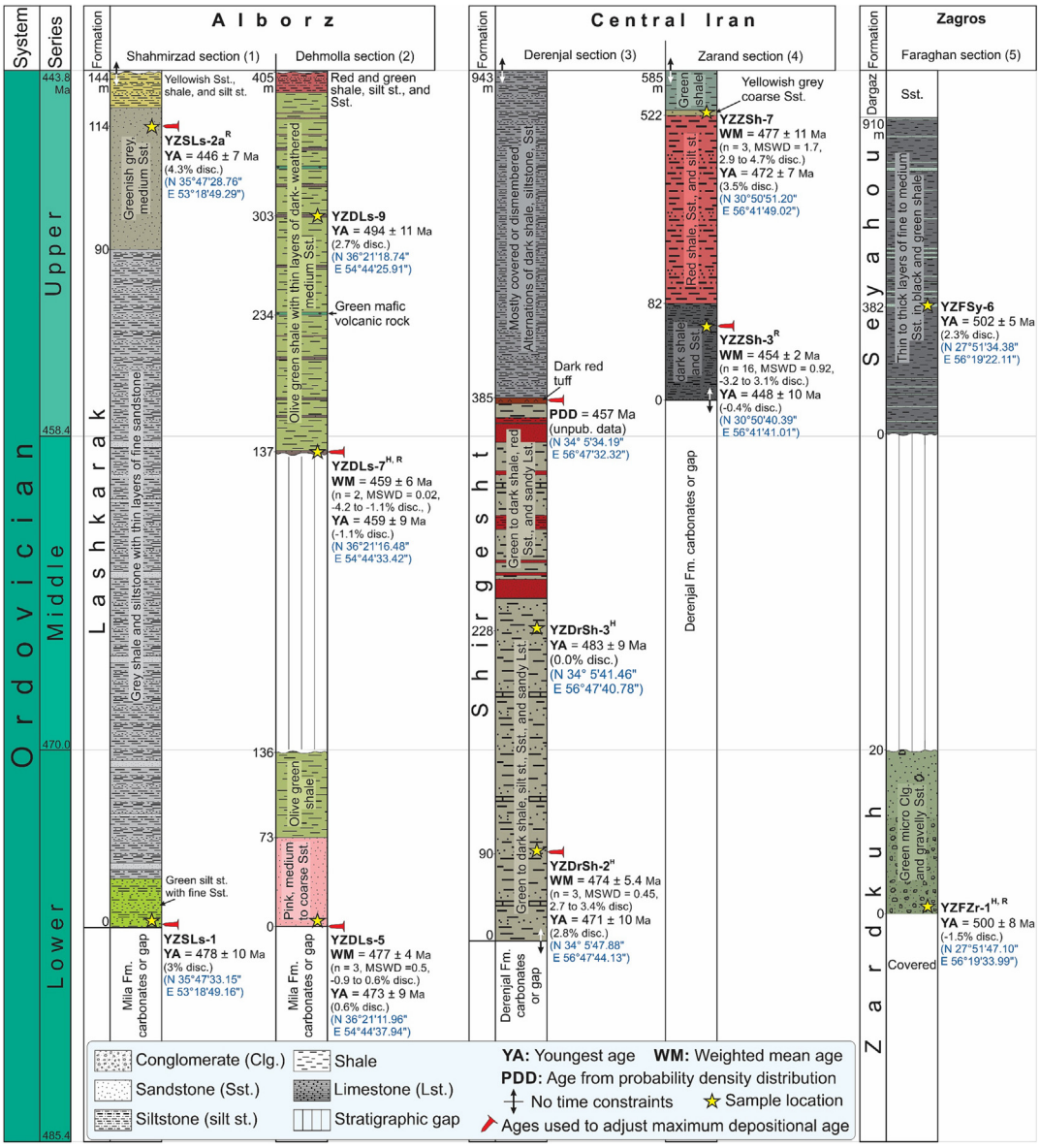

Fig. 3. Stratigraphic column of the Ordovician units of Iran in the studied sections showing dominant lithologies, stratigraphic gaps, geographic coordinates and stratigraphic locations of the samples. New detrital zircon U-Pb ages are obtained from all of the samples, and samples designated with "H" and "R" superscripts have been analyzed for detrital zircon Hf isotopes and detrital rutile U-Pb ages and trace elements, respectively. The youngest ages (YA) and weighted mean ages (WM) are calculated from detrital zircon U-Pb ages which are below ± 5 % discordant. Note that given the Ordovician depositional ages for these units are based on the fossil assemblages, the calculated ages from this study are used to calibrate the maximum depositional age of the sampled interval only if the new ages are not older than ages indicated by their fossil content. The samples used to calibrate the maximum depositional age of sediments are marked by a red pin. For samples with both youngest and weighted mean ages, the second age is used. The age given for the tuff layer in the middle part of the Shirgesht Formation, Derenjal section, is calculated from Probability Density Distribution (PDD) of zircon U-Pb ages (our unpublished data). The stratigraphic gaps in the Dehmolla and Faraghan sections are based on paleontological data and adapted from (Ghavidel-syooki, 2006; Ghobadi Pour et al., 2015; Ghobadi Pour, 2019; Ghavidel-Syooki, 2021). (For interpretation of the references to colour in this figure legend, the reader is referred to the web version of this article.)

robust approach is available for calculating original ages of discordant detrital grains due to lead-loss, we have filtered the detrital zircon U–Pb ages at 10 % discordance level. The discordant detrital zircon U–Pb data are not included in the data plots and interpretations, and only reported in the supplementary data files. However, in the case of detrital rutile U–Pb ages, the data pattern indicated discordance due to common-lead, from which corrected ages are calculated as explained in section 4.2, and no detrital rutile U–Pb data have been rejected using the discordance filter. For all concordant data, $^{206}Pb/^{238}U$ ages are used if younger than 1100 Ma, and $^{207}Pb/^{206}Pb$ ages are used if older than 1100 Ma. Kernel Density Estimation and Multidimensional Scaling diagrams were plotted using *IsoplotR* (Vermeesch, 2018).

4. Results

4.1. Detrital zircon and rutile morphology and internal structures

Detrital zircon grains in the Ordovician successions of Iran have morphologies ranging from angular to well-rounded, with bimodal distributions of angular to sub-angular and sub-rounded to well-rounded grains in most samples (supplementary Fig. 1). In CL images, the zircon grains show oscillatory and sector zoning, and core and rim structures (Fig. S2). Detrital rutile grains in these successions also have a wide range of morphologies but are mostly sub-rounded to well-rounded (Fig. S1). In BSE images, most rutile grains have homogenous internal textures. Detrital zircon and

detrital rutile grains for geochronology and geochemical analyses were selected from the different roundness classes according to their relative frequencies in each sample. Given that rims on the detrital zircons were generally too small to analyze, most measurements are from the core regions of the zircon grains.

4.2. Detrital zircon U–Pb–Hf

We divided the detrital zircon and rutile ages from each of the three Iranian blocks into four age intervals: (1) Pre-mid Stenian (> 1100 Ma) and (2) mid Stenian to early Ediacaran (1100 to 600 Ma), which are the dominant zircon age populations recorded in the Arabian-Nubian Shield, (3) middle Ediacaran—middle Cambrian (600 to 500 Ma) representing the age of the oldest crystalline rocks in Iran, and (4) late Cambrian—Ordovician (500—444 Ma), likely derived from local syn-sedimentary magmatic rocks.

4.2.1. Ordovician units in the Alborz block

Detrital zircon ages in five samples from the Lashkarak formation in Central Alborz (Shahmirzad and Dehmolla sections, respectively, sections number 1 and 2 in Fig. 1B) contain two dominant age fractions at 1100—600 Ma (28—57 % of the total populations, with age peaks at 940, 850, 810, 750, and 610 Ma) and 600—500 Ma (23—47 %; age peaks between 570 and 510 Ma) (Fig. 4A—E). Other minor age fractions include pre-Stenian ages (> 1100 Ma; 12—17 %), which range from 3300 to 2100 Ma (age peak at ca. 2500 Ma) and between 2100 and 1800 Ma, and ages between 500 and 446 Ma (4—16 %; Fig. 4A—E). In the Shahmirzad section, the two youngest ages (< ±5 % discordant) at 478 Ma (sample YZSLs-1) and 446 Ma (sample YZSLs-2a), provide maximum depositional ages for the base and near top of these strata, respectively (Fig. 3). In the Dehmolla section, weighted mean ages of 477 Ma (n = 3, MSWD = 0.5, sample YZDLs-5) and 459 Ma (n = 2, MSWD = 0.02, sample YZDLs-7) for the youngest grains provide maximum depositional ages for the base and middle part of these strata, respectively (Fig. 3).

Detrital zircon $\varepsilon Hf_{(t)}$ values from a sample (YZDLs-7) from the middle part of the Ordovician successions in east Central Alborz (Dehmolla section) range from −21.6 to +10.6 (Fig. 5A). The $\varepsilon Hf_{(t)}$ values in the detrital zircons older than 1100 Ma evolve from +8.4 at ca. 2700 Ma to −13.3 at ca. 1800 Ma. Detrital zircons in the major age fraction at 1100—600 Ma have variable $\varepsilon Hf_{(t)}$ values between −21.6 to +10.6, with the majority of grains (73 %) having positive $\varepsilon Hf_{(t)}$ values. The $\varepsilon Hf_{(t)}$ values of the 600—500 Ma age fraction range from −8 to +8.4. Ages younger than 500 Ma have $\varepsilon Hf_{(t)}$ values between −3.8 and +3.8 (Fig. 5A).

4.2.2. Ordovician units in the Central Iran block

Detrital zircon ages from the Ordovician Shirgesht Formation in the northern (samples YZDrSh-2 and 3) and southern (samples YZZSh-3 and 7) parts of the Central Iran block have similar age ranges, but with different frequencies for age fractions (Fig. 4). In the northern part of Central Iran (Derenjal section), 600—500 Ma grains comprise the dominant age fraction (54 % and 77 %; age peak at ca. 520 Ma), and 1100—600 Ma ages form the second most frequent age fraction (13 % and 29 %; minor age peaks at 950 and 690 Ma Fig. 4F and G). In the southern part of Central Iran (Zarand section), 1100—600 Ma grains form the major age fraction (48 % and 54 %; age peaks at ca. 950, 790, 775, and ca. 600 Ma), and 600—500 Ma grains form the second dominant age fraction (21 % and 31 %; age peaks at 545 Ma and 520 Ma). Grains between 500 and 445 Ma are less common (5—12 %) and form a shoulder of the main age peak in these samples (Fig. 4G and I). However, in sample YZZSh-3 from lower part of the formation in southern part of Central Iran (Zarand section), 500—445 Ma ages are more common (19 %) and form a prominent peak at 450 Ma (Fig. 3I). In both sections, ages older than 1100 Ma form minor age fractions (3—16 %) and are scattered between 3200 and 1800 Ma. Weighted mean ages of 474 Ma (n = 3, MSWD = 0.45, sample YZDrSh-2) and 454 Ma (n = 16, MSWD = 0.92, sample YZZSh-3) for the youngest grains, respectively, in the Derenjal and Zarand section provide maximum depositional ages for the lower part of these strata (Fig. 3).

Detrital zircon $\varepsilon Hf_{(t)}$ values for two samples from the Ordovician Shirgesht Formation in north Central Iran (YZDrSh-2 and 3) range from −18.9 to +9.6 (Fig. 5B). The $\varepsilon Hf_{(t)}$ values in the grains older than 1100 Ma are all sub-chondritic and range from −6.4 to −0.2. The 1100—600 Ma age fraction has more variable $\varepsilon Hf_{(t)}$ values from −18.9 to +8. The $\varepsilon Hf_{(t)}$ values in the major 600—500 Ma age fraction, and ages younger than 500 Ma are similar and range from −11.9 to +9.6, with the majority of grains having $\varepsilon Hf_{(t)}$ values from −4 to +3 (Fig. 5B).

4.2.3. Ordovician units in the Zagros block

Detrital zircons from two Ordovician units in the Zagros block have similar age ranges, but with different frequencies between age fractions. In the early Ordovician Zardkuh Formation (YZFZr-1), 600—500 Ma ages form the major age fraction (54 %; age peak at 530 Ma), and 1100—600 Ma ages are the second most frequent age fraction (23 %) with small age peaks at 800 and 610 Ma (and Fig. 4K). In the late Ordovician Seyahou Formation (YZFSy-6), the 1000—600 Ma ages are the dominant age fraction (59 %; a primary age peak at 610 Ma, a secondary age peak at 780 Ma, and minor age peaks at 1000 Ma and 880 Ma), and the 600—500 Ma ages form the second most frequent age fraction (30 %) and form a shoulder on the main age peak (Fig. 4J). Ages older than 1100 Ma form less common age fractions in both units (11 % and 22 %) and are scattered between 3300 and 1500 Ma with small age peaks at ca. 2500 Ma. Ages younger than 500 Ma are absent in these samples (Fig. 4J and K).

Detrital zircon $\varepsilon Hf_{(t)}$ values from the early Ordovician Zardkuh Formation (YZFZr-1) range from −21 to +9.1 (Fig. 5C). The $\varepsilon Hf_{(t)}$ values in detrital zircons older than 1100 Ma evolve from +2.8 at ca. 2500 Ma to −13.9 at ca. 1600 Ma (Fig. 5C). The 1100—600 Ma fraction has variable $\varepsilon Hf_{(t)}$ values ranging from −21 to +9.1. The $\varepsilon Hf_{(t)}$ values in the major age fraction at 600—500 Ma ranges from −5.7 to +5.2 with the majority of data points clustering between −3 and +4 (Fig. 5C).

4.3. Detrital rutile U–Pb

A significant portion (~60 %) of the detrital rutile ages in each sample are discordant (> ±10 % discordant) due to the variable incorporation of common-lead (Fig. S3). We calculate ^{207}Pb-corrected ages for these grains by measuring and correcting the common-Pb component based on Stacey and Kramers (1975) Pb-evolution model and using *IsoplotR* (Vermeesch, 2018). Accordingly, the KDE plots for each sample include two curves, which correspond to concordant ages (< ±10 % discordant; blue curve) and concordant + ^{207}Pb-corrected ages (red curve; Fig. 6). The concordant and discordant ages have similar age distributions for all samples, but in the concordant populations the frequencies of ages older than ca. 900 Ma are higher. This pattern likely reflects the higher radiogenic-lead content of the older grains and hence more concordant ages due to higher radiogenic/common lead ratios in these grains (Fig. 6). Therefore, to avoid bias induced by the concordance filter, we base our interpretations on the combined concordant and ^{207}Pb-corrected dataset (i.e., red curve; Fig. 6).

4.3.1. Ordovician successions in the Alborz block

Detrital rutile ages for two samples from the Lashkarak Formation in western (YZSLs-2a) and eastern (YZDLs-7) parts of Central

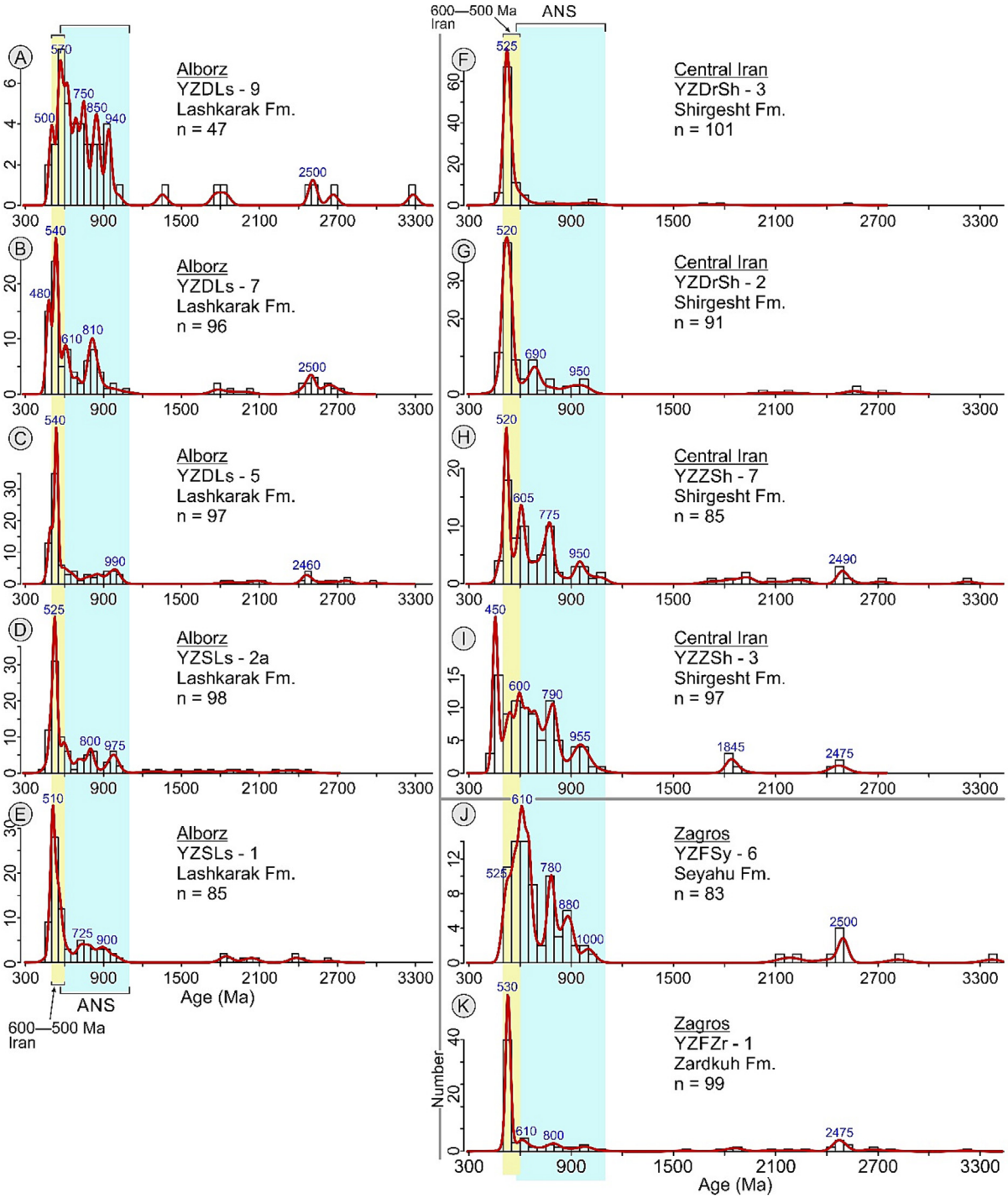

Fig. 4. Kernel Density Estimation (KDE) and histograms showing detrital zircon U–Pb ages from Ordovician siliciclastic successions in the Alborz (**A—E**), Central Iran (**F—I**), and Zagros (**J and K**) blocks. Histogram bin width is 50 Ma. Only concordant ages (< ±10 % discordant) are plotted. The pale blue band shows the age range of magmatism in the ANS, and the pale yellow band shows the age range of Ediacaran—middle Cambrian (600—500 Ma) magmatism in Iran. For source of data for the presented age ranges of the ANS crystalline basement and the Ediacaran—middle Cambrian magmatism in Iran see table 1 in supplementary file E. (For interpretation of the references to colour in this figure legend, the reader is referred to the web version of this article.)

Alborz show overlapping age ranges, but with different frequencies for age fractions (Fig. 6A and B). In the eastern part of Central Alborz (Dehmolla section), 600—500 Ma is the dominant detrital rutile age fraction (52 %; peak at 525 Ma), and the 1100—600 Ma ages form the second dominant age fraction (29 %; a peak at 640 Ma; Fig. 6A). In the western part of Central Alborz (Shahmirzad section), the 1100—600 Ma is the dominant age fraction (64 %; peak at 660 Ma), and 600—500 Ma forms a second dominant age fraction (18 %; a small peak at 570 Ma; Fig. 6B). Pre-1100 Ma grains comprise 13 % and 16 % of the population in each section, respectively, and scatter between 2600 and 1350 Ma (Fig. 6A and B). Both samples include rare ages between 500 and 457 Ma (2 % and 6 %).

4.3.2. Ordovician succession in the Central Iran block

Detrital rutile ages from the Shirgesht Formation in southern part of Central Iran block (YZZSh-3) include a major (74 %) age fraction at 1100—600 Ma (age peak at 630 Ma; Fig. 6C). The 600—500 Ma age fraction comprises 17 % of the population and forms

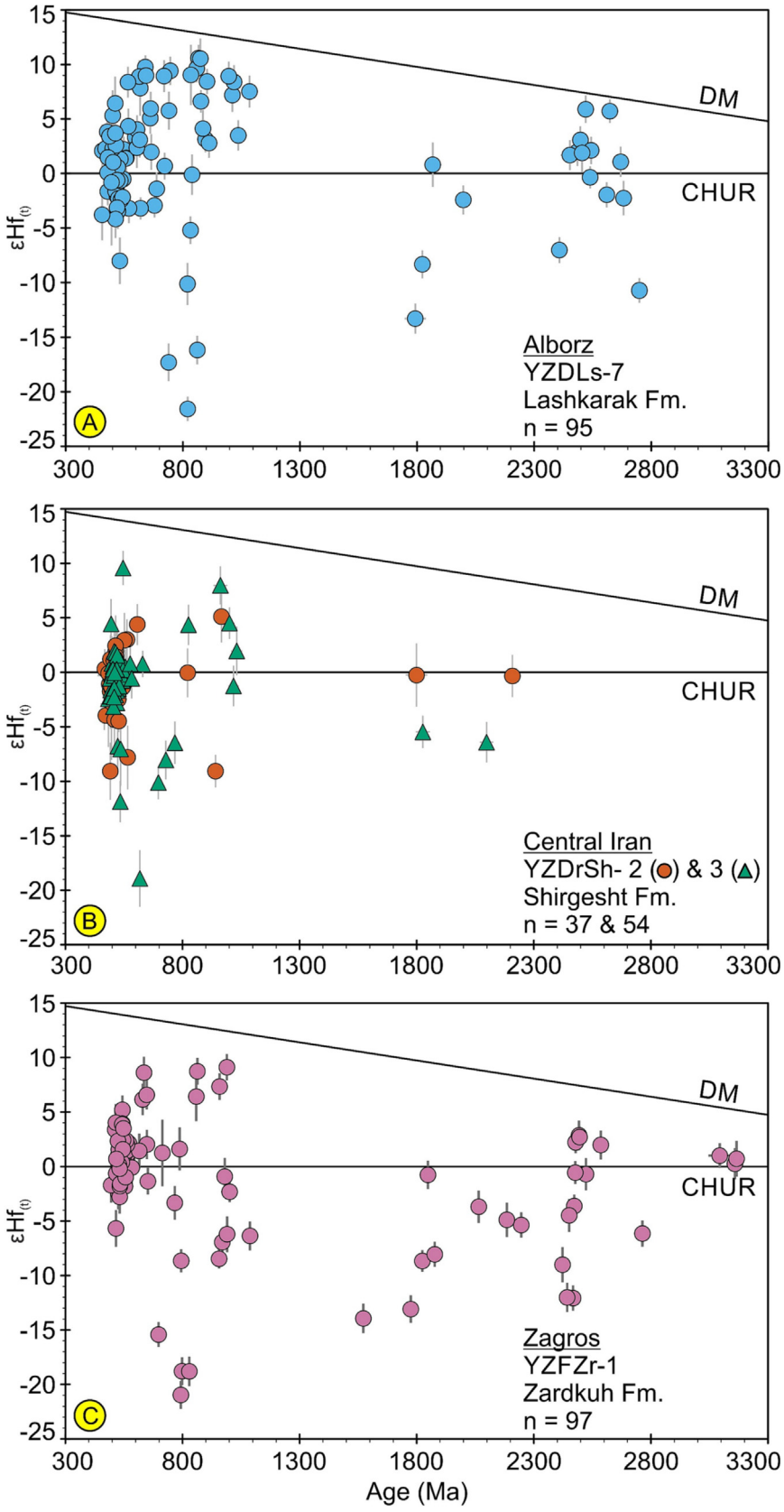

Fig. 5. $\varepsilon Hf_{(t)}$ values for detrital zircon grains from the Ordovician successions in the Alborz, Central Iran, and Zagros blocks. DM: depleted mantle (Vervoort and Blichert-Toft, 1999), CHUR: chondritic uniform reservoir (Bouvier et al., 2008). Error bars are 2 sigma.

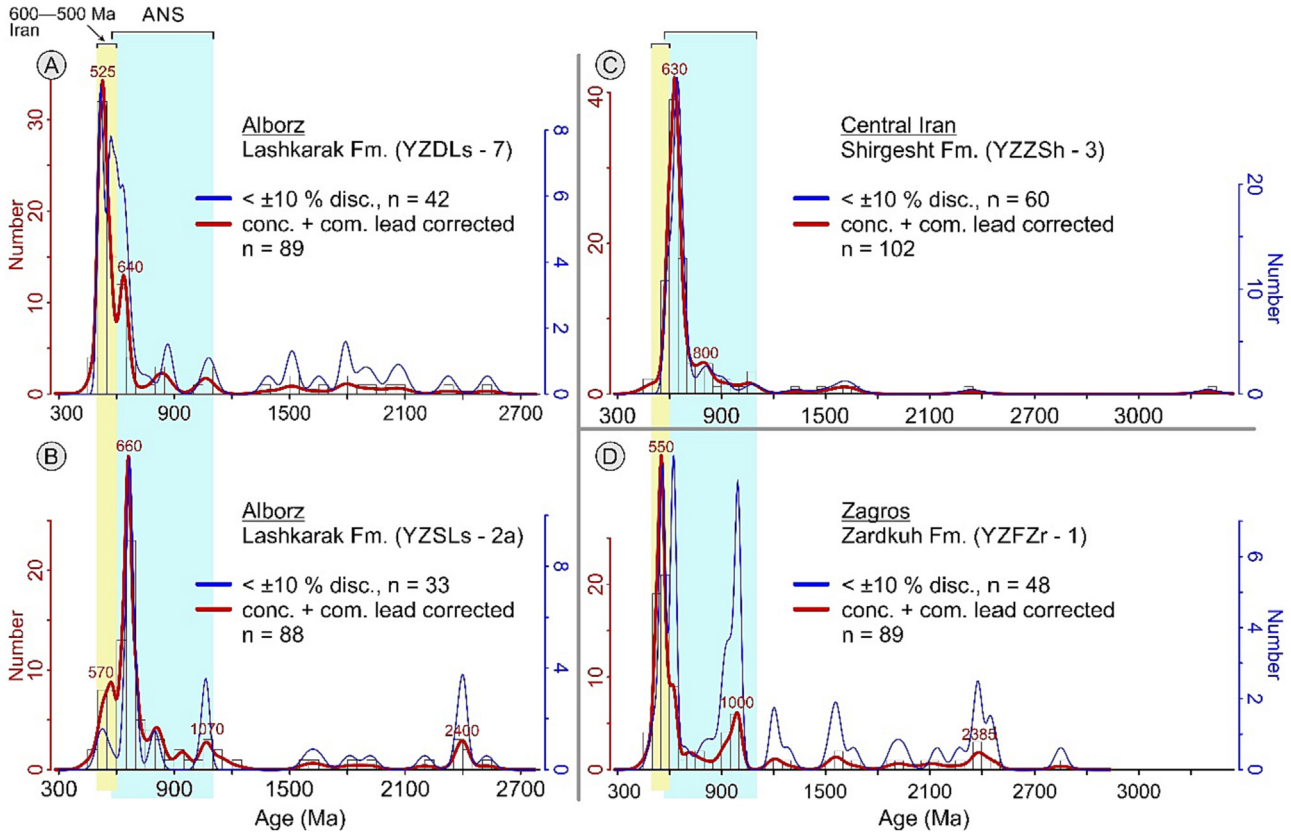

Fig. 6. KDE and histograms showing detrital rutile U–Pb ages from Ordovician successions in the Alborz, Central Iran, and Zagros blocks. Blue curves include concordant ages (< ±10 % discordant), and red curves include both concordant and common-lead corrected ages. Histograms only represent the red curves. The pale blue band indicates age range of magmatism in the ANS, and the pale yellow band indicates age range of Ediacaran—middle Cambrian (600—500 Ma) magmatism in the Iranian blocks. (For interpretation of the references to colour in this figure legend, the reader is referred to the web version of this article.)

the shoulder of the main age peak in the sample. Ages older than 1100 Ma represent 7 % of the population and are scattered between 3400 and 1300 Ma (Fig. 6C). The sample also includes a few (2 %) ages between 500 and 464 Ma.

4.3.3. Ordovician successions in the Zagros block

Detrital rutile ages in the early Ordovician Zardkuh Formation in Zagros (YZFZr-1) include a major (45 %) age fraction between 600 and 500 Ma forming a large age peak at 550 Ma. The 1100—600 Ma age fraction composes 30 % of the population and forms a small age peak at 1000 Ma (Fig. 6D). Ages older than 1100 Ma make up 20 % of the population and are scattered between 2900 and 1150 Ma (Fig. 6D). This unit also includes rare (4 %) ages between 500 and 454 Ma.

4.4. Detrital rutile trace elements

Crystallization temperatures for the detrital rutiles were calculated using the Zr-in-rutile thermometer calibration of Tomkins et al. (2007) at an assumed pressure of 5 kbar. Except for five outlier values between 950 and 1030 °C, calculated temperatures show similar ranges from ~380 °C to ~950 °C for the samples from the three blocks, which spans greenschist to granulite facies metamorphic conditions (Fig. 7). Among these, the majority (66 %) of grains in the four major age groups crystallized at temperatures of 550—750 °C (corresponding to amphibolite facies; Fig. 7). Most of the undatable detrital rutile grains (due to low U content and hence low radiogenic Pb ingrowth) yield lower crystallization temperatures of ~450 to ~650 °C.

Source rock lithologies of the detrital rutile were evaluated based on rutile Cr and Nb contents following the method of Triebold et al. (2012). The majority of detrital rutile grains in all age groups classify as being sourced from metapelitic/metafelsic lithologies (Fig. 8). Although the undatable detrital rutiles also follow this pattern, the frequency of rutile grains derived from metamafic sources are usually higher compared to dated rutile grains, which likely reflects the low U content of the rutile grains derived from mafic rocks (Zack and Kooijman, 2017)(Fig. 8).

Although a selection of other trace elements (Al, Sc, V, Mn, Fe, Co, Y, Mo, Sn, Hf, Ta, W, Pb, Th, U) were also measured, the provenance implications of these elements in detrital rutile are not well-constrained, and hence only briefly discussed here. Notable trends in these elements include strong positive correlation between Hf and calculated Zr-in-rutile temperatures, which reflects the similar geochemical behavior of Hf and Zr (cf., Luvizotto and Zack, 2009)). Additional trends include a correlation between crystallization temperatures and elemental concentrations with higher contents of V, Cr, Nb, Mo, Ta, Pb, and U, and lower contents of Sc, Co and Sn in detrital rutiles predicted to be derived from upper amphibolite and granulite-facies sources (cf., Agangi et al., 2020; Sciuba and Beaudoin, 2021). The data and plots for these trace elements are reported in supplementary file D and Fig. S4, respectively.

5. Discussion

5.1. Provenance of the Ordovician siliciclastic strata of Iran

Most proxies for continental reconstructions, including paleomagnetic and paleontological data, indicate the Iranian blocks

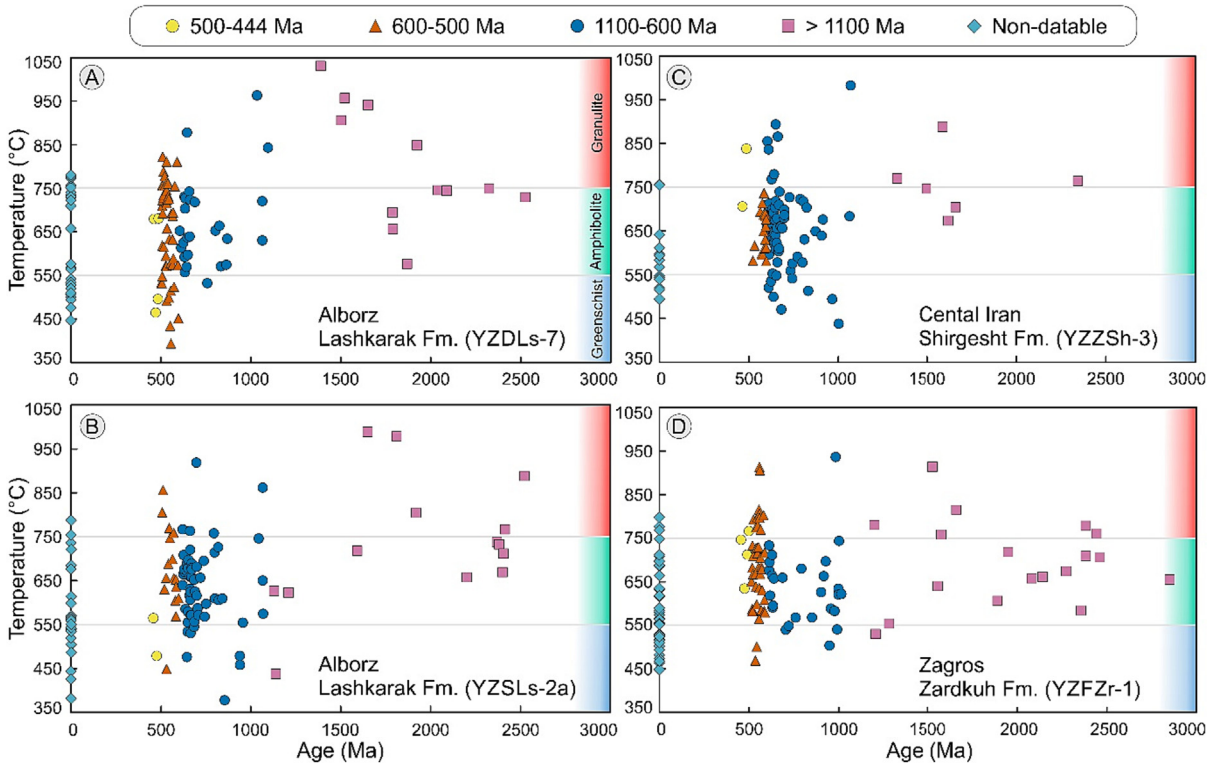

Fig. 7. Calculated crystallization temperatures for detrital rutile form Ordovician successions in the Alborz (A and B), Central Iran (C), and Zagros (D) blocks. The majority of the detrital rutile grains in all of the defined age fractions show crystallization temperatures of 550–750 °C. The undatable detrital rutiles (plotted at 0 Ma) mostly show lower crystallization temperatures of 450–650 Ma. Crystallization temperatures are calculated based on Zr content of the detrital rutile grains using the calibration of Tomkins et al. (2007) at 5 kbar.

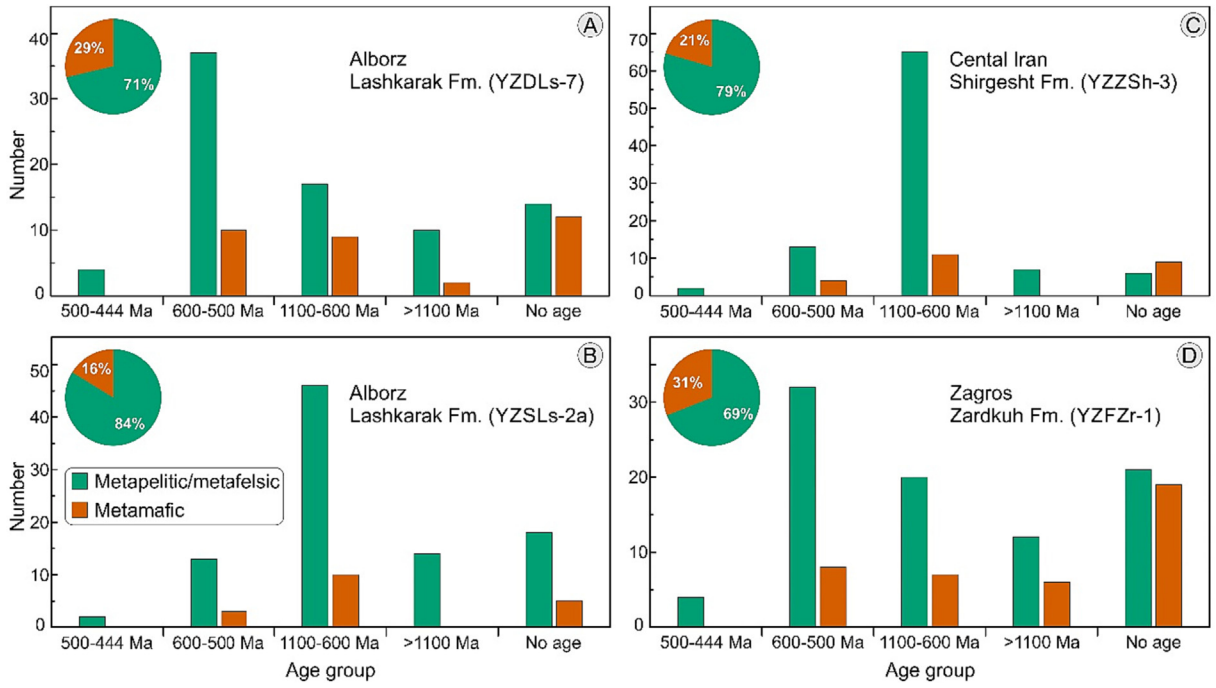

Fig. 8. Diagrams showing the proportions of detrital rutiles derived from metapelitic/metafelsic and metamafic sources in each age fraction (histograms) and the total populations in each sample (pie diagrams). Source rock lithologies are estimated based on the Cr-Nb discrimination method of Triebold et al. (2012).

were near the Arabian Plate along the northern margin of Gondwana from the Ediacaran to late Paleozoic (Becker et al., 1973; Soffel and Rster, 1980; Wensink, 1983; Vecoli and Le Hérissé, 2004; Ghavidel-syooki and Vecoli, 2008; Popov et al., 2015; Spina et al., 2020a; Ghavidel-Syooki, 2021). This location is further supported by provenance data from the Ediacaran–early Cambrian

siliciclastic strata of Iran that indicate a main source of detritus in the Neoproterozoic basement of the Arabian-Nubian Shield (ANS) (Horton et al., 2008; Etemad-Saeed et al., 2016; Honarmand et al., 2016; Chu et al., 2021; Shakerardakani et al., 2021; Zoleikhaei et al., 2021, 2022). Accordingly, in addition to the local basement of the Iranian blocks, the Ordovician basins of Iran may have also received detritus from more distal sources in the ANS. Below, we summarize our new data and compare them to previously published magmatic and metamorphic ages from these two potential source regions.

The detrital zircon and rutile U–Pb ages from Ordovician strata in Iran include two major age fractions at 1100—600 Ma (13—74 %) and 600—500 Ma (17—77 %), and two minor age fractions with one older than 1100 Ma (3—22 %) and the other at 500—444 Ma (0—19 %) (Figs. 4 and 6). The local basement of Iran does not include rocks older than 600 Ma, and hence provides no potential source rock for pre-600 Ma detrital zircon and rutile. The 1100—600 Ma and > 1100 Ma detrital zircon and rutile age fractions (with peaks at ca. 600 Ma, 800—700 Ma, and ca. 2500 Ma) are consistent with a source from the ANS basement, where there are widespread exposures of 1100—700 Ma (age peak at 800—700 Ma) arc terranes and syn-orogenic rocks and 700—570 Ma (age peak at 605 Ma) post-orogenic magmatic and metamorphic complexes (Fig. 9) (Hargrove et al., 2006a; Be'eri-Shlevin et al., 2009; Ali et al., 2010b; Morag et al., 2011; Ali et al., 2012; Be'eri-Shlevin et al., 2012; Abu El-Enen and Whitehouse, 2013; Eyal et al., 2014; Robinson et al., 2014; Yeshanew et al., 2015; Hassan et al., 2016; Whitehouse et al., 2016; Kozdrój et al., 2018; Robinson et al., 2018). The $\varepsilon Hf_{(t)}$ of the 1100—600 Ma detrital zircons are mostly (61 %) suprachondritic (Fig. 5), which is consistent with a source in the voluminous isotopically juvenile igneous rocks exposed in the basement of the ANS (95 % $\varepsilon Hf_{(t)}$ and 89 % $\varepsilon Nd_{(t)}$ > 0; Hargrove et al., 2006b; Be'eri-Shlevin et al., 2010; Morag et al., 2011; Robinson et al., 2014; Robinson et al., 2015; Ali et al., 2016; Gamal El Dien et al., 2021; Zoheir et al., 2021; Gamaleldien et al., 2022; Pease et al., 2022). Potential source rocks in the ANS for the less common (39 %) detrital zircons with subchondritic $\varepsilon Hf_{(t)}$ values include reworked Cryogenian-Ediacaran granitoid and gneissic rocks in the Khida, Abbas, Mahfid, and Eastern Desert terranes in southern and western parts of the ANS (Agar et al., 1992b; Windley et al., 1996; Whitehouse et al., 2001; Ali et al., 2013; Ali et al., 2015; Yeshanew et al., 2015; Yeshanew et al., 2017), and the widespread Cryogenian-Ediacaran glaciogenic successions covering the ANS, which contain Neoproterozoic detrital zircon with subchondritic $\varepsilon Hf_{(t)}$ values (Wilde and Youssef, 2002; Ali et al., 2010a; Nasiri Bezenjani et al., 2014; Fielding et al., 2017; Li et al., 2018; Abd El-Rahman et al., 2019). The ANS also includes potential sources for the detrital zircon and rutile grains older than 1100 Ma. These include crustal domains such as the Khida sub-terrane (ca. 1600 Ma; Agar et al., 1992a; Whitehouse et al., 2001), the Mahfid terrane in Yemen (ca. 2500 Ma; Windley et al., 1996; Whitehouse et al., 1998), or rocks of comparable ages in the Somalian and Ethiopian basement in the southern part of the ANS, and eastern part of the Sahara Metacraton (Sultan et al., 1994; Kröner and Sassi, 1996; Teklay et al., 1998; Abdelsalam et al., 2002; Bea et al., 2011; Stern et al., 2012). The Cr and Nb contents of the detrital rutile grains older than 600 Ma indicate that the majority of these grains were derived from metapelitic/metafelsic rocks and less commonly from metamafic rocks (Fig. 8), which is consistent with the intermediate to felsic basement of the ANS with minor mafic–ultramafic ophiolites along the suture zones of the arc terranes (Johnson et al., 2004). The calculated crystallization temperatures of detrital rutile grains older than 600 Ma range from ~450 to ~950 °C, with most temperatures between 550 and 750 °C (Fig. 7), also support a source in the typically greenschist to amphibolite facies, and less common granulite facies, metamorphic rocks in the ANS basement (e.g., Johnson and Woldehaimanot, 2003; Hargrove, 2006; Johnson et al., 2011; Al-Saleh, 2012; Fritz et al., 2013; El-Sawy and El-Shafei, 2019).

Alternatively, the detrital zircon and rutile grains in the Ordovician units with source signatures from the ANS could be recycled from the underlying Ediacaran—early Cambrian siliciclastic units of Iran. These Ediacaran—early Cambrian successions are themselves interpreted to be sourced from the ANS (Horton et al., 2008; Etemad-Saeed et al., 2016; Honarmand et al., 2016; Zoleikhaei et al., 2021, 2022), and their detrital rutile and zircon age peaks and $\varepsilon Hf_{(t)}$ values are similar to the 1100—600 Ma and > 1100 Ma age fractions in the Ordovician units (Fig. 9 and Zoleikhaei et al., 2021).

Although the ANS includes a few small exposures of rocks as young as 520 Ma, its crystalline rock record is dominantly older than 600 Ma and hence pre-dates the major 600—500 Ma age fraction in the Ordovician successions of Iran. A more likely source for these 600—500 Ma detrital zircon and rutile grains are the local 600 to 500 Ma plutons exposed in the Iranian basement (Fig. 9) (e.g., Ramezani and Tucker, 2003; Hassanzadeh et al., 2008; Balaghi Einalou et al., 2014; Rossetti et al., 2015; Honarmand et al., 2018; Sepidbar et al., 2020; Shafaii Moghadam et al., 2020a; Moghadam et al., 2021). The $\varepsilon Hf_{(t)}$ values for the 600—500 Ma detrital zircon grains in the Ordovician units range from −11.9 to +9.6 (Fig. 5), which is similar to the magmatic zircon $\varepsilon Hf_{(t)}$ and whole-rock $\varepsilon Nd_{(t)}$ data from the Ediacaran—middle Cambrian magmatic rocks of Iran (91 % $\varepsilon Hf_{(t)}$ and 95 % $\varepsilon Nd_{(t)}$ between −10 to +10; Nutman et al., 2013; Balaghi Einalou et al., 2014; Chiu et al., 2017; Honarmand et al., 2018; Daneshvar et al., 2019; Asadi Sarshar et al., 2020; Mehdipour Ghazi et al., 2020; Sepidbar et al., 2020; Shafaii Moghadam et al., 2020a; Moghadam et al., 2021; Nouri et al., 2021; Gholipour et al., 2022; Nouri et al., 2022) and hence further supports a local source for 600—500 Ma detritus. The Cr-Nb systematics of the 600—500 Ma detrital rutiles indicate that the majority of these grains are derived from metapelitic/metafelsic and less commonly from metamafic source rocks, which is consistent with the dominance of felsic rocks in the 600—500 Ma magmatic complexes in Iran. The crystallization temperatures for the these detrital rutiles mostly range between 550 and 750 °C (Fig. 7), which is also consistent with the amphibolite-facies metamorphism experienced by some Ediacaran—middle Cambrian granitoids in Iran (Balaghi Einalou et al., 2014). Alternatively, the 600—500 Ma detrital rutile grains could have been derived from unexposed metapelitic units in the basement of Iran into which the 600—500 Ma granitoids intrude. In this scenario, the 600—500 Ma detrital rutile grains may be derived from metapelites confined to the contact aureoles of 600—500 Ma granitoids or record a regional metamorphic event associated with 600—500 Ma plutonism. We favor the latter interpretation because these grains are ubiquitous in Ordovician strata sampled over an extensive area of Iran (Fig. 1B, 2, and 6).

The Ediacaran—middle Cambrian plutonism in Iran diminished by 520 Ma (Fig. 9) and was followed by a less-intense pulse of magmatism during the Ordovician—Silurian. This later phase of magmatism provides a potential local source for the 500—444 Ma detrital zircons and rare detrital rutile grains in Ordovician strata. These rocks include rare plutons of early Ordovician to late Silurian age (483—425 Ma) (Ghavidel-Syooki et al., 2011b; Fergusson et al., 2016; Moghadam et al., 2017a; Ranjbar Moghadam et al., 2018; Shirdashtzadeh et al., 2018; Vesali et al., 2020; Samadi et al., 2022) and intercalations of 468—441 Ma mafic to felsic volcanic rocks within the middle to upper Ordovician successions in the Alborz and Central Iran blocks (Bagheri and Stampfli, 2008; Derakhshi and Ghasemi, 2015; Derakhshi et al., 2017; Fatehi and Ahmadipour, 2018; Derakhshi et al., 2022). The $\varepsilon Hf_{(t)}$ values for

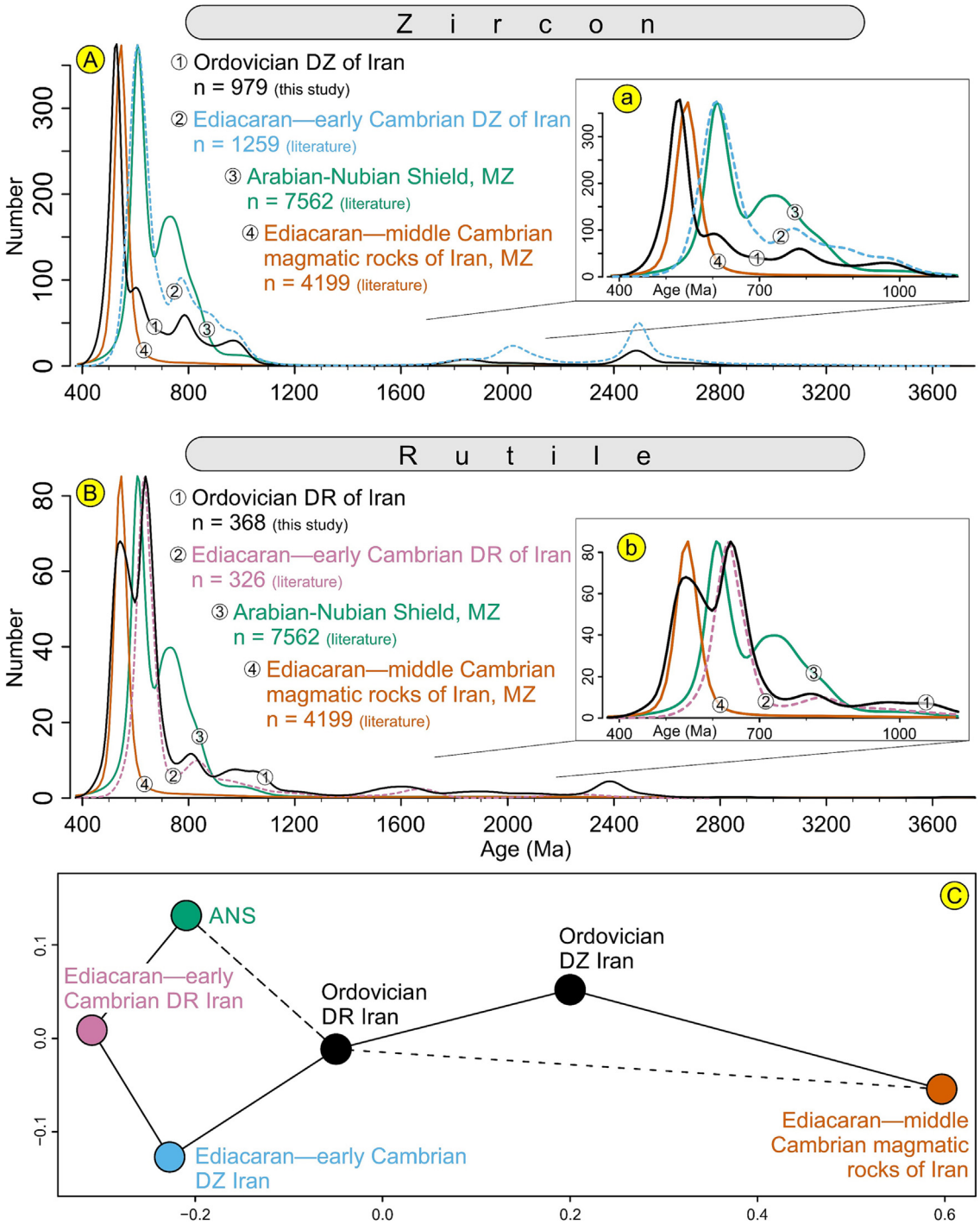

Fig. 9. KDE plots (A and B) and Multidimensional Scaling (MDS) plot (C) comparing detrital zircon and rutile ages from Ordovician siliciclastic successions of Iran to detrital zircon and rutile ages from Ediacaran—early Cambrian siliciclastic strata of Iran (Horton et al., 2008; Etemad-Saeed et al., 2016; Honarmand et al., 2016; Chu et al., 2021; Zoleikhaei et al., 2021), and magmatic zircon ages from the Arabian-Nubian Shield (ANS) and Ediacaran—middle Cambrian (600—500 Ma) magmatic rocks of Iran. Solid lines on the MDS plot show nearest neighbor, dashed lines show next nearest neighbor. For source of data from the ANS and Ediacaran—middle Cambrian (600—500 Ma) magmatic rocks of Iran see table 1 in supplementary file E. DZ: detrital zircon, DR: detrital rutile, MZ: magmatic zircon.

500—444 Ma detrital zircons in the Ordovician units range from −9.1 to +4.4 with the majority (93 %) of values between −4 and +4 (Fig. 5), which is compatible with the isotopic composition of the Ordovician magmatism in Iran (whole-rock $\varepsilon Nd_{(t)}$ = −1.4 to +4.5 and zircon $\varepsilon Hf_{(t)}$ = +2.5 to +8.2; Derakhshi et al., 2017; Moghadam et al., 2017a; Vesali et al., 2020). The tectonothermal event associated with the Ordovician magmatism in Iran could also have produced potential sources for the rare (0—5 %) detrital rutile grains younger than 500 Ma. Detrital rutile Cr and Nb contents suggest that all of the 500—444 Ma rutile grains are derived from metapelitic/metafelsic rocks (Fig. 8). These could have been sourced from metapelites or metafelsic rocks in parts of the unexposed metamorphic basement of Iran that were thermally overprinted during Ordovician—Silurian magmatism.

In summary, the detrital zircon and rutile provenance record of Ordovician strata in Iran suggest sources in local crystalline base-

ment and Ediacaran—early Cambrian sedimentary units and potentially more distal sources in the Arabian-Nubian Shield in the Gondwanan hinterland. However, given the proximal sources in the local basement in Iran for 600—444 Ma detrital zircon and rutile grains, and the revised model for Ordovician sedimentary basins of Iran (sections 5.2 and 5.3), it is more likely that detrital zircon and rutile grains with ages corresponding with the ANS basement (> 600 Ma) in these successions are also recycled from the underlying Ediacaran—early Cambrian siliciclastic successions in the local basement and not directly derived from the ANS.

5.2. Basin paleogeography

Although our new data indicate that 600—500 Ma plutonic rocks in Iran were an important sediment source for local Ordovician basins, the underlying Ediacaran—early Cambrian siliciclastic strata appear to have been sourced solely from the ANS (Zoleikhaei et al., 2021, 2022). These findings suggest that the 600—500 Ma magmatic rocks in Iran had little or no surface expression during the Ediacaran—early Cambrian (i.e., no volcanic units) and were instead emplaced as intrusions into an actively subsiding basement. The appearance of prominent 600—500 Ma detrital zircon and detrital rutile age populations in the Ordovician strata of Iran suggests exposure and erosion of the 600—500 Ma plutons, marking a distinct change in basin evolution. In addition to the new provenance data, a major change in the evolution of sedimentary basins along the NMG between the Cambrian and Ordovician is independently supported by several aspects of the Ordovician geology of Iran: (1) The Ordovician in Iran marks the reappearance of terrigenous sediments after an interval of carbonate deposition (Fig. 2) (i.e., the middle to late Cambrian Mila Formation and equivalent units; Ruttner et al., 1968; Bruton et al., 2004; Ghavidel-syooki, 2006; Ghavidel-syooki and Vecoli, 2008; Asghari, 2014; Geyer et al., 2014; Ghavidel- Syooki, 2019; Ghorbani, 2019; Bayet-Goll et al., 2022b). These thick carbonate sequences, together with the underlying highly mature quartz-rich sandstones (top unit of the Lalun Formation, Fig. 2) are interpreted to reflect a peneplained source area (i.e., ANS) and diminished terrigenous sediment production during the Cambrian (Zoleikhaei et al., 2022). (2) Detrital mode and whole-rock chemical analyses reflect an immature composition for most of the Ordovician sandstones of Iran, which has been interpreted to support tectonic reactivation in the source area (Bayet-Goll, 2014; Khazaei et al., 2018; Jazimagh et al., 2020; Bayet-Goll et al., 2022b). An exception to the generally immature composition of Ordovician sandstones may include the laterally-discontinuous, submature arkosic sandstones observed at the base of the Lashkarak Formation in the Dehmolla section, Central Alborz. (3) Unlike the underlying Cambrian units, the Ordovician successions are not laterally continuous across the Iranian blocks and they might include significant stratigraphic gaps or be completely absent in different areas of the same block (Stampfli et al., 1991; Ghavidel-syooki, 1994b, 2006; Ghobadi Pour et al., 2011; Asghari, 2014; Ghavidel-Syooki et al., 2014; Vennin et al., 2015; Ghavidel-syooki, 2017; Ghavidel-Syooki, 2021; Álvaro et al., 2022). The lateral discontinuity and unconformable contacts of these strata are associated with synsedimentary normal faults and partial erosion of the underlying Cambrian successions, which is interpreted to indicate deposition in fault-bound basins associated with block tilting (e.g., Álvaro et al., 2022; Bayet-Goll et al., 2022b). Accordingly, we suggest that active uplift in Iran during the Ordovician exposed 600—500 Ma plutons and their enclosing country rock, resulting in a shift in sedimentary provenance to local sources. This contrasts with the stable platform setting and distal ANS source of the underlying Ediacaran and Cambrian strata in Iran.

Faulting and basement uplift could have been caused by either compressional or extensional tectonics. However, the normal sense of movement for the synsedimentary faults in the Ordovician successions indicate extensional tectonism (Álvaro et al., 2022; Bayet-Goll et al., 2022b; Bayet-Goll et al., 2023). In addition, the mafic alkaline to sub-alkaline volcanic rocks in the Ordovician successions have geochemical affinities with transitional to within-plate volcanism and are consistent with continental rift-related setting (Mehdizadeh Shahri, 2008; Derakhshi and Ghasemi, 2015; Derakhshi et al., 2017; Ranjbar Moghadam et al., 2018; Derakhshi et al., 2022).

5.3. Implications for Paleozoic extension in Iran

Ordovician extensional tectonism in Iran has traditionally been interpreted to mark the initiation of Paleo-Tethys rifting in northern Gondwana (Stöcklin, 1974; Stampfli et al., 1991). Detachment of an outboard (micro-)continental block accompanied by domal uplift and normal faulting could account for the regional tectonic rejuvenation, and the formation of fault-bound basins and alkaline mafic volcanism observed in the Ordovician geology of Iran. However, in the context of opening of the Paleo-Tethys, several details of the record of Paleozoic extension in Iran remain poorly understood including: (1) the duration of rifting, (2) the architecture of the rift zone including the location of the rift axis, and (3) the identity of any rifted (micro-)continental block(s). Resolving these unknowns is important for refining tectonic models for the Paleozoic evolution of the NMG and the opening of the Paleo-Tethys.

Stampfli et al. (1991) proposed an Ordovician—Silurian opening of the Paleo-Tethys in the Iranian segment of the NMG based on the occurrence of Ordovician—Silurian mafic volcanic rocks in the Alborz block. However, other works have advocated for a much younger opening of the Paleo-Tethys in this region based on the observation that rift-related magmatic activity in Iran extended throughout the middle and late Paleozoic (e.g., Bagheri and Stampfli, 2008; Karimpour et al., 2010; Saccani et al., 2013; Derakhshi and Ghasemi, 2014; Derakhshi et al., 2017; Mohammadi et al., 2020). Paleozoic volcanic rocks occur as subaerial and submarine flows of alkaline to sub-alkaline basalt and andesite intercalating with Ordovician to Carboniferous sedimentary successions (Mahmudy Gharaie et al., 2004; Aharipour et al., 2010; Ayati et al., 2010; Torabi and Hashemi, 2010; Valinasab Zarnagh et al., 2022). The contemporaneous plutonic rocks include gabbroic rocks of alkaline and oceanic basalt (MORB) geochemical affinities with subsidiary A-type granitic rocks, which intrude into the older basement of Iran and have isotopic ages ranging from 483 Ma to 351 Ma (Saccani et al., 2013; Rahimi–Chakdel and Raghimi, 2014; Ranjbar Moghadam et al., 2018; Shirdashtzadeh et al., 2018; Shahsavari Alavijeh et al., 2019; Golestani, 2020; Mohammadi et al., 2020; Vesali et al., 2020; Sepidbar et al., 2023).

The thickest accumulation of Ordovician—Silurian mafic volcanic rocks occurs in northeastern Iran, which are spatially associated with Permo-Triassic ophiolitic mélanges, and are generally interpreted to mark the axis of Paleo-Tethys rifting (Figs. 1 and 10) (Stampfli et al., 1991). However, similar Ordovician—Silurian alkaline mafic volcanic rocks and late Paleozoic—early Mesozoic ophiolitic mélanges and ultramafic rocks (e.g., Anarak-Jandaq and Posht-e-Badam ophiolitic mélanges, and Takab complex) are also found within the Alborz and Central Iran blocks, well inboard of the proposed Paleo-Tethys rifting and suture zone (Fig. 10) (Bagheri and Stampfli, 2008; Zanchi et al., 2009b; Kargaranbafghi et al., 2012; Masoodi et al., 2013; Zanchi et al., 2015; Khalili et al., 2016; Gharibnejad et al., 2020; Gyomlai et al., 2022). Although the Anarak-Jandaq ophiolitic mélange is interpreted to have been displaced from an original position near the Paleo-Tethys suture in NE Iran based on lithostratigraphic and paleomag-

netic evidence (Fig. 10) (Davoudzadeh and Weber-Diefenbach, 1987; Soffel et al., 1996; Mattei et al., 2012; Mattei et al., 2015), this interpretation cannot easily account for other within-block ophiolitic mélanges away from the Paleo-Tethys suture zone. Furthermore, remnants of early to middle Paleozoic extensional basins are preserved in Central Iran that are filled with thick sequences of continental detritus and mafic flows, which document continued continental extension inboard of the inferred rift axis of the Paleo-Tethys Ocean (Fig. 10) (e.g., the Kashmar-Kerman Tectonic Zone, southern Sanandaj-Sirjan Zone, and northern margin of Yazd block; Ruttner et al., 1968; Daneshmand, 1995; Masoodi et al., 2013; Hairapetian et al., 2015; Fatehi and Ahmadipour, 2018). Accordingly, the distribution of early—middle Paleozoic mafic volcanic rocks (i.e., evidence of extension), and late Paleozoic-early Mesozoic ophiolites (i.e., evidence of closure of the extensional zones) in the Iranian blocks suggests that the early Paleozoic extension in Iran was widespread across the different blocks, rather than confined to a narrow rift axis in northeast Iran.

If long-lived Paleozoic extension in Iran lead to the opening of the Paleo-Tethys along this sector of the NMG through detachment of a (micro-)continental block, the thick accumulation of Ordovician—Silurian extensional volcanic rocks in northeastern Iran represents the most likely location of continental break-up. A rift axis in northeast Iran is consistent with paleogeographic proxies that indicate that the Iranian blocks remained attached to Gondwana after the inferred opening of the Paleo-Tethys Ocean during the Paleozoic (e.g., Soffel et al., 1996; Besse et al., 1998; Horton et al., 2008; Muttoni et al., 2009a; Muttoni et al., 2009b; Ghavidel-syooki, 2017; Spina et al., 2020a; Spina et al., 2020b; Ghavidel-Syooki, 2021). Thus, the opening of the Paleo-Tethys Ocean would require detachment of continental blocks outboard (north) of Iran along the NMG. However, recent data shows that peri-Gondwanan blocks now scattered throughout central and eastern Asia (Karakum, Tarim, Tianshan, Tibet, Qaidam, Qiangtang, Qilian, North-China), were not located near Iran and Anatolia as assumed in earlier reconstructions of the Paleo-Tethys margins (Stampfli et al., 1991; Stampfli and Borel, 2002). Instead, these blocks have closer affinities with northern India and Australia (Fig. 1A) (e.g., Wang et al., 2020; Cawood et al., 2021; Wei et al., 2022). Gondwanan blocks accreted to the southern margin of Eurasia are generally interpreted to have been derived directly from the opposing margin of northern Gondwanan without significant lateral transfer as they drifted northward (e.g., Wang et al., 2020; Cawood et al., 2021; Metcalfe, 2021; Wei et al., 2022). The Turan Block is located immediately to the north of the Paleo-Tethys suture in NE Iran (present-day position; Fig. 10) and hence is the most obvious candidate block to have rifted from Iran during the opening of the Paleo-Tethys. Nonetheless, the Turan Block is interpreted to be a collage of Paleozoic—Jurassic arcs that were formed on the southern margin of Eurasia and then juxtaposed through strike-slip movement (Garzanti and Gaetani, 2002; Natal'in and Şengör, 2005). The Turan Block therefore appears to have little affinity with the Proterozoic basement and thick Paleozoic cover sequences that characterize the geology of Iran.

Although the identity of any continental block(s) that may have rifted from northern Iran during the development of the Paleo-Tethys remains unknown, the new detailed record of Ordovician rifting in Iran presented here, particularly the distinct change in basin evolution and provenance between Ediacaran-Cambrian and Ordovician strata, provides a new geological 'piercing point' to identify formerly contiguous continental blocks. However, given that a suitable continental block has yet to be identified, a plausible alternative hypothesis is that Paleozoic extension in Iran was not related to successful rifting of an outboard continental terrane. Instead, given that the Ediacaran—Cambrian succession in Iran indicate a transitional to marginal marine depositional basin

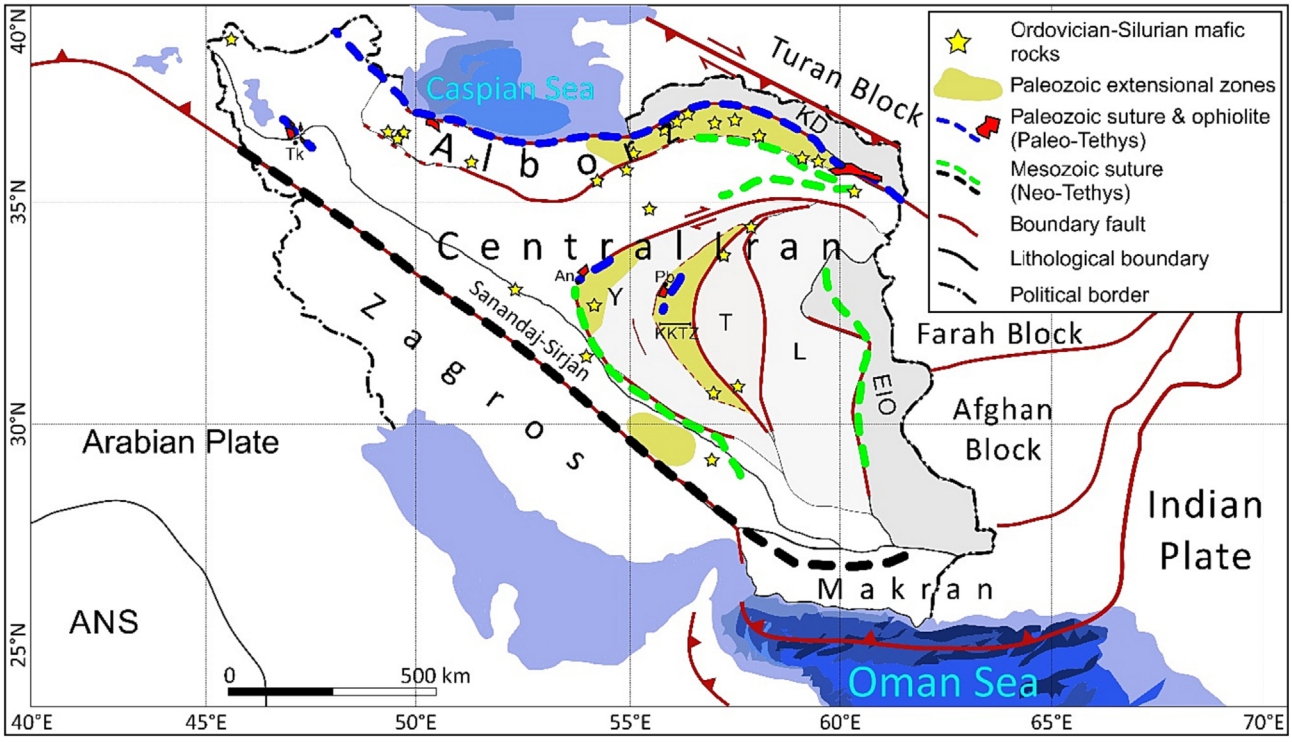

Fig. 10. Geological map of Iran showing main structural blocks, bounding faults, oceanic sutures and ophiolite belts, and Ordovician—Silurian mafic volcanic rocks. Note that Paleo-Tethys related ophiolites are found in several locations inboard of the main rift axis and suture zone of the ocean in NE Iran. Locations of Ordovician—Silurian mafic volcanic rocks are from Derakhshi et al. (2022). Y: Yazd block, T: Tabas block, L: Lut block, UDMA: Urumieh-Dokhtar Magmatic Arc, KD: Kopet Dagh; KKTZ: Kashmar-Kerman Tectonic Zone, EIO: East Iranian Orocline, An: Anarak, Pb: Posht-e-Badam, Tk: Takab.

(e.g., Berberian and King, 1981; Sharland et al., 2001; Al-Husseini, 2010), this segment of the NMG may have already faced an ocean that was established during the Ediacaran—Cambrian and post-Cambrian extension in Iran was related to extension in a continental margin. Based on the present-day distribution of Ordovician rift-related deposits, the Ordovician extensional zone in Iran may have been up to 800 km wide and comparable in size to extensional zones such as the Basin and Range Province, the Iberian Margin, or the West Antarctic Rift (Buck, 1991; Behrendt, 1999; Cunha, 2008; Salerno et al., 2016). Fig. 11 outlines a possible model for Ordovician extensional tectonism and sedimentation in Iran based on our new data and those from the literature. Ordovician extension formed fault-bound basins restricted by uplifted and tilted blocks (i.e., in the form of horst and graben structures) in this segment of the NMG that was accompanied by deposition of compositionally immature sediments and mafic magmatism (Fig. 11). Sediments were sourced locally from uplifted regions (horsts) containing Ediacaran—Cambrian successions along with exposures of 600—500 Ma magmatic rocks (Fig. 11). Therefore, in our model, the 'ANS-aged' detrital zircon and detrital rutile present in most of the Ordovician formations were recycled from underlaying Ediacaran—early Cambrian siliciclastic strata, which also contain these age fractions. Different frequencies of 1100—600 Ma and 600—500 Ma age fractions in the detrital zircon and detrital rutile datasets (Figs. 4 and 6) indicate variations in the exposed areas of different source components (i.e., the 600—500 Ma plutonic rocks and the Ediacaran—early Cambrian cover strata) in each region. The ophiolitic mélanges inland form the inferred Paleo-Tethys rift axis and the associated early—middle Paleozoic continental to marine sedimentary depocenters indicate that the extensional zones (i.e., the grabens) within Iranian blocks formed narrow rift-basins that may have locally developed a floor of oceanic lithosphere. However, given the ophiolites between the Iranian blocks are generally scarce (Fig. 10), it is unlikely that these rift basins developed long-lived spreading centers. The continued extension in the Iranian blocks from early to late Paleozoic suggests that the wide extensional zone initiated during the Ordovician may have been periodically active until at least late Paleozoic. The Ediacaran—Ordovician oceanic basin to the north of Iran may have lasted through to the late Paleozoic when the Neo-Tethys Ocean opened as the Alborz and Central Iran blocks rifted away from northern Gondwana. We continue to use the name Paleo-Tethys for this ocean, which is the ocean that existed before the Neo-Tethys in this segment of the NMG.

5.4. Ordovician history of the northern margin of Gondwana

The tectonic regime of the northern margin of Gondwana during the Ordovician was not uniform across the length of the margin. To the east of Iran along the northern margin of Gondwana, in northern India and Australia, closure of the Proto-Tethys Ocean was underway in early Paleozoic and was completed by the late Silurian as several Asian blocks (e.g., North China, South China, Tarim, Qaidam, North Qiangtang, and Indochina) collided with the Gondwana during the Bhimphedian Orogeny (Cawood et al., 2007; Metcalfe, 2021). The Bhimphedian Orogeny was followed by post-collisional extension and opening of the Paleo-Tethys Ocean during the Silurian, which carved off several continental blocks (e.g., North China, South China, Tarim, Qaidam, North Qiangtang, and Indochina) from the northern margin of Gondwana (Metcalfe, 2021). To the west of Iran along the NMG, in northern Africa and South America, compressional tectonism during the Cadomian Orogeny related to the southward subduction of the Iapetan oceanic crust and associated arc magmatism and arc-continent collision, was underway during the Neoproterozoic—Cambrian (ca. 540 Ma) (Nance et al., 2010; Cawood et al., 2021). During the Ordovician, continued subduction of the Iapetus oceanic crust initiated post-collisional extension in the margin, which led to the opening of the Rheic Ocean and detachment of Avalonia and Carolinia from the Gondwana margin (Nance et al., 2010). The Rheic Ocean continued spreading until late Silurian. Therefore, during the early Paleozoic, intensive extension related to opening of the Rheic Ocean in the western segment of the NMG was changing eastward into compressional tectonism related to the closure of the Proto-Tethys Ocean in the eastern segment of the NMG. Iran occupied a link between eastern and western segments of the NMG and the Ordovician—Silurian extension recorded in the Iranian blocks indicate that they had a closer affinity to the extensional tectonism in the western segment of the NMG. In this context, the oceanic crust to the north of Iran likely belonged to the Rheic oceanic plate rather than the southward subducting Proto-Tethys oceanic plate.

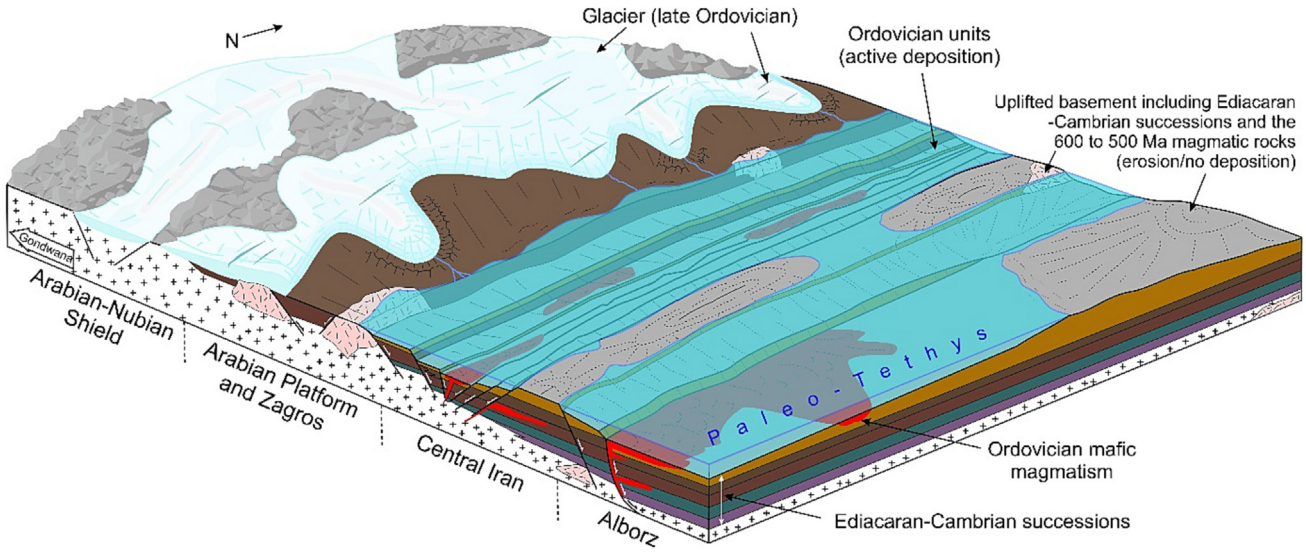

Fig. 11. Schematic model of the northern margin of Gondwanan during the Ordovician. Active extension led to formation of horst and graben structures and mafic magmatism. Uplifted regions experienced erosion or non-deposition, whereas nearby extensional basins record nearly continuous sedimentation from Ediacaran to Ordovician. Note that the glaciers only appeared in the late Ordovician.

6. Conclusions

Integrated provenance data including detrital zircon U–Pb age and Hf isotopes and detrital rutile U–Pb age and trace elements from Ordovician siliciclastic successions across the Iranian blocks indicate derivation from local basement and recycling from Ediacaran—early Cambrian siliciclastic strata in Iran, with some possible additional input from the Arabian-Nubian shield in the Gondwanan hinterland. Exposure of the 600—500 Ma magmatic rocks in the Iranian basement and extensive unconformities in Ordovician sequences suggest widespread exposure of local basement in the vicinity of Ordovician extensional basins, which are marked by thick successions of compositionally immature siliciclastic strata and mafic volcanic rocks. The new data support a marked change in basin style in Iran from a laterally extensive, epicontinental basin in the Ediacaran—Cambrian that was infilled with distally-sourced detritus, to compartmentalized deposition in actively extending narrow depocenters during the Ordovician with detritus sourced from local uplifts. The Ordovician extension in Iran is traditionally interpreted to indicate detachment of a continental block from northern Iran and opening of the Paleo-Tethys Ocean. However, the continental block to the north of Iran in the NMG has yet to be identified and the Paleozoic extension in Iran temporally and spatially extends beyond the preferred age and location of the Paleo-Tethys rift, respectively. Therefore, the Ordovician geology of Iran may reflect a broad zone of extension developed across an established Ediacaran-Cambrian continental margin and was not associated with the successful rifting of an outboard block. The tectonic regime of the northern margin of Gondwana during early Paleozoic varied along its length, and the Ordovician—Silurian extensional tectonism developed in Iran had a closer association with the contemporaneous extensional tectonism and opening of the Rheic Ocean in the western segment of the NMG than compressional tectonism and subduction of the Proto-Tethys Ocean in the eastern segment of the NMG.

CRediT authorship contribution statement

Yousef Zoleikhaei: Conceptualization, Methodology, Formal analysis, Investigation, Data curation, Writing – original draft, Writing – review & editing, Visualization. **Jacob A. Mulder:** Conceptualization, Formal analysis, Resources, Writing – original draft, Writing – review & editing. **Peter A. Cawood:** Validation, Funding acquisition, Supervision, Writing – review & editing, Supervision.

Declaration of competing interest

The authors declare that they have no known competing financial interests or personal relationships that could have appeared to influence the work reported in this paper.

Acknowledgments

This paper forms part of the PhD project of Yousef Zoleikhaei, which was supported by a PhD scholarship from Monash University and Australian Research Council grant FL160100168. The authors thank Younes Zoleikhaei, Mohammad Zoleikhaei and Rashid Zoleikhaei for their help in fieldwork and sample shipment. Massimo Raveggi, Rachelle Pierson, and Junnel Alegado from Monash University are thanked for assisting with laboratory analyses. We extend our gratitude to Aram Bayet-Goll for his constructive review and Inna Safonova for efficient editorial handling.

Appendix A. Supplementary material

Supplementary data to this article can be found online at https://doi.org/10.1016/j.gr.2023.10.017.

References

Abd El-Rahman, Y., Abu Anbar, M., Li, X.-H., Li, J., Ling, X.-X., Wu, L.-G., Masoud, A.E., 2019. The evolution of the Arabian-Nubian Shield and survival of its zircon U-Pb-Hf-O isotopic signature: A tale from the Um Had Conglomerate, central Eastern Desert Egypt. Precambrian Res. 320, 46–62. https://doi.org/10.1016/j.precamres.2018.10.011.

Abdelsalam, M.G., Liégeois, J.-P., Stern, R.J., 2002. The Saharan Metacraton. J. Afr. Earth Sci. 34 (3), 119–136. https://doi.org/10.1016/S0899-5362(02)00013-1.

Abu El-Enen, M.M., Whitehouse, M.J., 2013. The Feiran-Solaf metamorphic complex, Sinai, Egypt: Geochronological and geochemical constraints on its evolution. Precambrian Res. 239, 106–125. https://doi.org/10.1016/j.precamres.2013.10.011.

Agangi, A., Plavsa, D., Reddy, S.M., Olierook, H., Kylander-Clark, A., 2020. Compositional modification and trace element decoupling in rutile: Insight from the Capricorn Orogen Western Australia. *Precambrian Res.* 345,. https://doi.org/10.1016/j.precamres.2020.105772 105772.

Agar, R. A., Stacey, J. S., & Whitehouse, M. J. (1992a). Archaean to lateProterozoic evolution of the southern Afif terrane, Kingdom of Saudi Arabia: a study using Sm–Nd and ion-probe U–Pb zircon geochronology. Saudi Arabian Directorate General of Mines & Geology, Open file report OF-10-15.

Agar, R. A., Stacey, J. S., & Whitehouse, M. T. (1992b). *Evolution of the southern Afif terrane — a geochronologic study*. Jiddah, Saudi Arabia: Directorate General of Mineral Resources, Open File Report DGMR-OF-10-15.

Agard, P., Omrani, J., Jolivet, L., Whitechurch, H., Vrielynck, B., Spakman, W., MoniÉ, P., Meyer, B., Wortel, R., 2011. Zagros orogeny: a subduction-dominated process. Geol. Mag. 148 (5–6), 692–725. https://doi.org/10.1017/S001675681100046X.

Aghanabati, A., Rezaei, A., 2009. Correlation of lithostratigraphic units of Iran in major structural-sedimentary basins. Geological Society of Iran.

Aharipour, R., Moussavi, M.R., Mosaddegh, H., Mistiaen, B., 2010. Facies features and paleoenvironmental reconstruction of the Early to Middle Devonian syn-rift volcano-sedimentary succession (Padeha Formation) in the Eastern-Alborz Mountains. NE Iran. *Facies* 56 (2), 279–294. https://doi.org/10.1007/s10347-009-0200-x.

Al-Husseini, M.I., 2010. MIDDLE EAST GEOLOGIC TIME SCALE 2010: Early Cambrian Asfar Sequence. Geoarabia 15 (1), 137–160.

Ali, K.A., Stern, R.J., Manton, W.I., Johnson, P.R., Mukherjee, S.K., 2010a. Neoproterozoic diamictite in the Eastern Desert of Egypt and Northern Saudi Arabia: evidence of ~750 Ma glaciation in the Arabian-Nubian Shield? Int. J. Earth Sci. 99 (4), 705–726. https://doi.org/10.1007/s00531-009-0427-3.

Ali, K.A., Stern, R.J., Manton, W.I., Kimura, J.-I., Whitehouse, M.J., Mukherjee, S.K., Johnson, P.R., Griffin, W.R., 2010b. Geochemical, U-Pb zircon, and Nd isotope investigations of the Neoproterozoic Ghawjah Metavolcanic rocks. Northwestern Saudi Arabia. *Lithos* 120 (3), 379–392. https://doi.org/10.1016/j.lithos.2010.08.024.

Ali, K.A., Andresen, A., Manton, W.I., Stern, R.J., Omar, S.A., Maurice, A.E., 2012. U-Pb zircon dating and Sr–Nd–Hf isotopic evidence to support a juvenile origin of the ~ 634 Ma El Shalul granitic gneiss dome. Arabian-Nubian Shield. *Geol. Mag.* 149 (5), 783–797. https://doi.org/10.1017/S0016756811000975.

Ali, K.A., Wilde, S.A., Stern, R.J., Moghazi, A.-K.-M., Ameen, S.M.M., 2013. Hf isotopic composition of single zircons from Neoproterozoic arc volcanics and post-collision granites, Eastern Desert of Egypt: Implications for crustal growth and recycling in the Arabian-Nubian Shield. Precambrian Res. 239, 42–55. https://doi.org/10.1016/j.precamres.2013.05.007.

Ali, K.A., Kröner, A., Hegner, E., Wong, J., Li, S.-Q., Gahlan, H.A., Abu El Ela, F.F., 2015. U-Pb zircon geochronology and Hf–Nd isotopic systematics of Wadi Beitan granitoid gneisses, South Eastern Desert. Egypt. *Gondwana Res.* 27 (2), 811–824. https://doi.org/10.1016/j.gr.2013.11.002.

Ali, K.A., Zoheir, B.A., Stern, R.J., Andresen, A., Whitehouse, M.J., Bishara, W.W., 2016. Lu–Hf and O isotopic compositions on single zircons from the North Eastern Desert of Egypt, Arabian-Nubian Shield: Implications for crustal evolution. Gondwana Res. 32, 181–192. https://doi.org/10.1016/j.gr.2015.02.008.

Al-Saleh, A.M., 2012. The Kirsh gneiss dome: an extensional metamorphic core complex from the SE Arabian Shield. Arab. J. Geosci. 5 (2), 335–344. https://doi.org/10.1007/s12517-010-0179-1.

Álvaro, J.J., Ghobadi Pour, M., Sánchez-García, T., Kebria-ee Zadeh, M.-R., Hairapetian, V., Popov, L.E., 2022. Stratigraphic and volcanic signatures of Miaolingian-Late Ordovician rift pulses in the Alborz Mountains, northern Iran. J. Asian Earth Sci. 233,. https://doi.org/10.1016/j.jseaes.2022.105240 105240.

Asadi Sarshar, M., Moghadam, H.S., Griffin, W.L., Santos, J.F., Stern, R.J., Ottley, C.J., Sarkarinejad, K., Sepidbar, F., O'Reilly, S.Y., 2020. Geochronology and geochemistry of exotic blocks of Cadomian crust from the salt diapirs of SE Zagros: the Chah-Banu example. Int. Geol. Rev. 1–22. https://doi.org/10.1080/00206814.2020.1787236.

Asghari, A., 2014. Sedimentary environment, sequence stratigraphy and paleogeography of Paleozoic Pre-Khuff succession in southern Iran (Zagros

and Persian Gulf) Retrieved from Université De Bourgogne https://theses.hal.science/tel-01134278 (2014DIJOS058.
Ayati, F., Khalili, M., Noghreyan, M., Mackizade, M.A., 2010. The Silurian magmatism in the Abyane –Soh area (Kashan-Central Iran). J. Sci. Univ. Tehran (no Publish) 35 (4), 21–31.
Azizi, H., Whattam, S.A., 2022. Does Neoproterozoic-Early Paleozoic (570–530 Ma) basement of Iran belong to the Cadomian Orogeny? Precambrian Res. 368,. https://doi.org/10.1016/j.precamres.2021.106474 106474.
Bagheri, S., Stampfli, G.M., 2008. The Anarak, Jandaq and Posht-e-Badam metamorphic complexes in central Iran: New geological data, relationships and tectonic implications. Tectonophysics 451 (1), 123–155. https://doi.org/10.1016/j.tecto.2007.11.047.
Balaghi Einalou, M., Sadeghian, M., Zhai, M., Ghasemi, H., Mohajjel, M., 2014. Zircon U-Pb ages, Hf isotopes and geochemistry of the schists, gneisses and granites in Delbar Metamorphic-Igneous Complex, SE of Shahrood (Iran): Implications for Neoproterozoic geodynamic evolutions of Central Iran. J. Asian Earth Sci. 92, 92–124. https://doi.org/10.1016/j.jseaes.2014.06.011.
Barber, D.E., Stockli, D.F., Horton, B.K., Koshnaw, R.I., 2018. Cenozoic Exhumation and Foreland Basin Evolution of the Zagros Orogen During the Arabia-Eurasia Collision. Western Iran. *Tectonics* 37 (12), 4396–4420. https://doi.org/10.1029/2018TC005328.
Bayet-Goll, A., 2022. Ordovician matground and mixground ecosystems in shoreface–offshore and barrier-island environments from Central Iran, northern Gondwana. Geol. Mag. 159 (6), 925–953. https://doi.org/10.1017/S0016756822000097.
Bayet-Goll, A., Carvalho, C., 2017. Sedimentological and ichnological characteristics of deltaic and non-deltaic successions of the Lower Ordovician of Shahmirzad area, Alborz mountains of northern Iran. Boll. Soc. Paleontol. Ital. 56 (2), 127–151. https://doi.org/10.4435/BSPI.2017.17.
Bayet-Goll, A., Chen, J., Moussavi-Harami, R., Mahboubi, A., 2015. Depositional processes of ribbon carbonates in Middle Cambrian of Iran (Deh-Sufiyan Formation, Central Alborz). Facies 61 (3). https://doi.org/10.1007/s10347-015-0436-6.
Bayet-Goll, A., Neto de Carvalho, C., 2016. Ichnology and sedimentology of a tide-influenced delta in the Ordovician from the northeastern Alborz range of Iran (Kopet Dagh region). Lethaia 49 (3), 327–350. https://doi.org/10.1111/let.12150.
Bayet-Goll, A., Myrow, P.M., AceÑOlaza, G.F., Moussavi-Harami, R., Mahboubi, A., 2016. Depositional Controls on the Ichnology of Ordovician Wave-dominated Marine Facies: New Evidence from the Shirgesht Formation. Central Iran. *Acta Geol. Sin.* 90 (5), 1572–1597. https://doi.org/10.1111/1755-6724.12803.
Bayet-Goll, A., Geyer, G., Daraei, M., 2018. Tectonic and eustatic controls on the spatial distribution and stratigraphic architecture of late early Cambrian successions at the northern Gondwana margin: The siliciclastic-carbonate successions of the Lalun Formation in central Iran. Mar. Pet. Geol. 98, 199–228. https://doi.org/10.1016/j.marpetgeo.2018.08.002.
Bayet-Goll, A., Buatois, L.A., Mángano, M.G., Daraei, M., 2022a. The interplay of environmental constraints and bioturbation on matground development along the marine depositional profile during the Ordovician Radiation. Geobiology 20 (2), 233–270. https://doi.org/10.1111/gbi.12473.
Bayet-Goll, A., Sharafi, M., Jazimagh, N., Brandano, M., 2022b. Understanding along-strike variability in controlling mechanisms of paleoenvironmental conditions and stratigraphic architecture: Ordovician successions in the Alborz Mountains of Iran at the northern Gondwana margin. Mar. Pet. Geol. 140,. https://doi.org/10.1016/j.marpetgeo.2022.105654 105654.
Bayet-Goll, A., Sharafi, M., Daraei, M., Nasiri, Y., 2023. The influence of hybrid sediment gravity flows on distribution and composition of trace-fossil assemblages: Ordovician succession of the north-eastern Alborz Range of Iran. Sedimentology 70 (3), 783–827. https://doi.org/10.1111/sed.13058.
Bayet-Goll, A. (2014). *Ichnology and sequence stratigraphy Mila Formation (Central Alborz) and comparsion with Shirgesht Formation (Tabas block).* (PhD), Frdowsi University of mashhad, Retrieved from https://library.um.ac.ir/index.php?option=com_lib&view=docinfo&type=2&DocID=55936&lang=fa.
Be'eri-Shlevin, Y., Katzir, Y., Blichert-Toft, J., Kleinhanns, I. C., & Whitehouse, M. J. (2010). Nd–Sr–Hf–O isotope provinciality in the northernmost Arabian–Nubian Shield: implications for crustal evolution. *Contrib. Mineral. Petrol., 160*(2), 181-201. doi:10.1007/s00410-009-0472-8.
Bea, F., Montero, P., Anbar, M.A., Talavera, C., 2011. SHRIMP dating and Nd isotope geology of the Archean terranes of the Uweinat-Kamil inlier, Egypt–Sudan–Libya. Precambrian Res. 189 (3), 328–346. https://doi.org/10.1016/j.precamres.2011.07.017.
Becker, H., Förster, H., Soffel, H., 1973. Central Iran, a former part of Gondwanaland? Paleomagnetic evidence from Infracambrian rocks and iron ores of the Bafq area, Central Iran. Z. Geophys. 39, 953–963.
Be'eri-Shlevin, Y., Katzir, Y., Whitehouse, M., 2009. Post-collisional tectonomagmatic evolution in the northern Arabian-Nubian Shield: time constraints from ion-probe U-Pb dating of zircon. J. Geol. Soc. 166 (1), 71. https://doi.org/10.1144/0016-76492007-169.
Be'eri-Shlevin, Y., Eyal, M., Eyal, Y., Whitehouse, M.J., Litvinovsky, B., 2012. The Sa'al volcano-sedimentary complex (Sinai, Egypt): A latest Mesoproterozoic volcanic arc in the northern Arabian Nubian Shield. Geology 40 (5), 403–406. https://doi.org/10.1130/G32788.1.
Behrendt, J.C., 1999. Crustal and lithospheric structure of the West Antarctic Rift System from geophysical investigations — a review. Global Planet. Change 23 (1), 25–44. https://doi.org/10.1016/S0921-8181(99)00049-1.
Berberian, M., King, G.C.P., 1981. Towards a paleogeography and tectonic evolution of Iran. Can. J. Earth Sci. 18 (2), 210–265. https://doi.org/10.1139/e81-019.
Besse, J., Torcq, F., Gallet, Y., Ricou, L.E., Krystyn, L., Saidi, A., 1998. Late Permian to Late Triassic palaeomagnetic data from Iran: constraints on the migration of the Iranian block through the Tethyan Ocean and initial destruction of Pangaea. Geophys. J. Int. 135 (1), 77–92. https://doi.org/10.1046/j.1365-246X.1998.00603.x.
Bouvier, A., Vervoort, J.D., Patchett, P.J., 2008. The Lu–Hf and Sm–Nd isotopic composition of CHUR: Constraints from unequilibrated chondrites and implications for the bulk composition of terrestrial planets. Earth Planet. Sci. Lett. 273 (1), 48–57. https://doi.org/10.1016/j.epsl.2008.06.010.
Bruton, D., Wright, A., Hamedi, M., 2004. Ordovician Trilobites from Iran. Palaeontogr. Abt. A Palaozool. - Stratigr. 271 (5–6), 111–149. https://doi.org/10.1127/pala/271/2004/111.
Buck, W.R., 1991. Modes of continental lithospheric extension. J. Geophys. Res. Solid Earth 96 (B12), 20161–20178. https://doi.org/10.1029/91JB01485.
Cawood, P.A., Johnson, M.R.W., Nemchin, A.A., 2007. Early Palaeozoic orogenesis along the Indian margin of Gondwana: Tectonic response to Gondwana assembly. Earth Planet. Sci. Lett. 255 (1), 70–84. https://doi.org/10.1016/j.epsl.2006.12.006.
Cawood, P.A., Martin, E.L., Murphy, J.B., Pisarevsky, S.A., 2021. Gondwana's interlinked peripheral orogens. Earth Planet. Sci. Lett. 568,. https://doi.org/10.1016/j.epsl.2021.117057 117057.
Chiu, H.-Y., Chung, S.-L., Zarrinkoub, M.H., Melkonyan, R., Pang, K.-N., Lee, H.-Y., Wang, K.-L., Mohammadi, S.S., Khatib, M.M., 2017. Zircon Hf isotopic constraints on magmatic and tectonic evolution in Iran: Implications for crustal growth in the Tethyan orogenic belt. J. Asian Earth Sci. 145, 652–669. https://doi.org/10.1016/j.jseaes.2017.06.011.
Chu, Y., Wan, B., Allen, M.B., Chen, L., Lin, W., Talebian, M., Xin, G., 2021. Detrital Zircon Age Constraints on the Evolution of Paleo-Tethys in NE Iran: Implications for Subduction and Collision Tectonics. Tectonics 40 (8). https://doi.org/10.1029/2020TC006680.
Clark-Lowes, D.D., 2005. Arabian glacial deposits: recognition of palaeovalleys within the Upper Ordovician Sarah Formation, Al Qasim district. Saudi Arabia. *Proc. Geol. Assoc.* 116 (3), 331–347. https://doi.org/10.1016/S0016-7878(05)80051-3.
Cunha, T., 2008. Gravity anomalies, flexure and the thermo-mechanical evolution of the West Iberia Margin and its conjugate of Newfoundland. University of Oxford. PhD),Retrieved from.
Daneshmand, V., 1995. *Report of 1: 100 '0000 geological map of sheet 7351 - Zara*nd Retrieved from Geological Survey of Iran (in Persian) http://www.ngdir.ir/down/1441; http://www.ngdir.ir/down/1440.
Daneshvar, N., Maanijou, M., Azizi, H., Asahara, Y., 2019. Petrogenesis and geodynamic implications of an Ediacaran (550 Ma) granite complex (metagranites), southwestern Saqqez, northwest Iran. J. Geodyn. 132,. https://doi.org/10.1016/j.jog.2019.101669 101669.
Davoudzadeh, M., Weber-Diefenbach, K., 1987. Contribution to the paleogeography, stratigraphy and tectonics of the Upper Paleozoic of Iran. Neues Jahrb. Geol. Palaontol. Abhand. 175 (2), 121–146.
Derakhshi, M., Ghasemi, H., 2014. Ordovician-Devonian magmatism in the north of Shahrood: implication for long lived rifting of Paleotethys in eastern Alborz. Petrolog. J. 5 (18), 105–122.
Derakhshi, M., Ernst, R.E., Kamo, S.L., 2022. Ordovician-Silurian volcanism in northern Iran: Implications for a new Large Igneous Province (LIP) and a robust candidate for the Late Ordovician mass extinction. Gondwana Res. 107, 256–280. https://doi.org/10.1016/j.gr.2022.03.009.
Derakhshi, M., Ghasemi, H., 2015. Soltan Maidan Complex (SMC) in the eastern Alborz structural zone, northern Iran: magmatic evidence for Paleotethys development. Arab. J. Geosci. 8 (2), 849–866. https://doi.org/10.1007/s12517-013-1180-2.
Derakhshi, M., Ghasemi, H., Miao, L., 2017. Geochemistry and petrogenesis of Soltan Maidan basalts (E Alborz, Iran): Implications for asthenosphere-lithosphere interaction and rifting along the N margin of Gondwana. Geochemistry 77 (1), 131–145. https://doi.org/10.1016/j.chemer.2017.01.002.
Ebbestad, J.O.R., Ghobadi Pour, M., Bassett, M.G., Popov, L.E., 2016. First occurrence of Lesueurilla prima (Gastropoda) from the Middle Ordovician (Darriwilian) of Iran. GFF 138 (4), 510–518. https://doi.org/10.1080/11035897.2016.1186110.
El-Sawy, E.-S.-K., El-Shafei, M.K., 2019. Geometric and tectonic analysis of Ad-Damm mega-scale fold: implication of Neoproterozoic Transpressive Regime in the west-central Arabian Shield. Arab. J. Geosci. 12 (7), 224. https://doi.org/10.1007/s12517-019-4391-3.
Etemad-Saeed, N., Hosseini-Barzi, M., Adabi, M.H., Miller, N.R., Sadeghi, A., Houshmandzadeh, A., Stockli, D.F., 2016. Evidence for ca. 560Ma Ediacaran glaciation in the Kahar Formation, central Alborz Mountains, northern Iran. Gondwana Res. 31, 164–183. https://doi.org/10.1016/j.gr.2015.01.005.
Evans, D.H., Ghobadi Pour, M., Popov, L.E., 2013. Review of the Early to Mid Ordovician orthoconic cephalopods from Iran. Bull. Geosci. 88 (1), 21–44. https://doi.org/10.3140/bull.geosci.1355.
Eyal, M., Be'eri-Shlevin, Y., Eyal, Y., Whitehouse, M.J., Litvinovsky, B., 2014. Three successive Proterozoic island arcs in the Northern Arabian-Nubian Shield: Evidence from SIMS U-Pb dating of zircon. Gondwana Res. 25 (1), 338–357. https://doi.org/10.1016/j.gr.2013.03.016.
Fatehi, H., Ahmadipour, H., 2018. Geochemistry and petrogenesis of metabasites from the gol-e-gohar complex in southern sanandaj-sirjan metamorphic zone, south of iran; evidences for crustal extension and magmatism at early

palaeozoic. Geol. Acta 16 (3), 293–319. https://doi.org/10.1344/GeologicaActa2018.16.3.4.
Fergusson, C.L., Nutman, A.P., Mohajjel, M., Bennett, V.C., 2016. The Sanandaj-Sirjan Zone in the Neo-Tethyan suture, western Iran: Zircon U-Pb evidence of late Palaeozoic rifting of northern Gondwana and mid-Jurassic orogenesis. Gondwana Res. 40, 43–57. https://doi.org/10.1016/j.gr.2016.08.006.
Fielding, L., Najman, Y., Millar, I., Butterworth, P., Ando, S., Padoan, M., Barfod, D., Kneller, B., 2017. A detrital record of the Nile River and its catchment. J. Geol. Soc. 174 (2), 301. https://doi.org/10.1144/jgs2016-075.
Fritz, H., Abdelsalam, M., Ali, K.A., Bingen, B., Collins, A.S., Fowler, A.R., Ghebreab, W., Hauzenberger, C.A., Johnson, P.R., Kusky, T.M., Macey, P., Muhongo, S., Stern, R.J., Viola, G., 2013. Orogen styles in the East African Orogen: A review of the Neoproterozoic to Cambrian tectonic evolution. J. Afr. Earth Sci. 86, 65–106. https://doi.org/10.1016/j.jafrearsci.2013.06.004.
Gamal El Dien, H., Li, Z.-X., Abu Anbar, M., Doucet, L.S., Murphy, J.B., Evans, N.J., Xia, X.-P., Li, J., 2021. Two-stage crustal growth in the Arabian-Nubian shield: Initial arc accretion followed by plume-induced crustal reworking. Precambrian Res. 359,. https://doi.org/10.1016/j.precamres.2021.106211 106211.
Gamaleldien, H., Li, Z.-X., Abu Anbar, M., Murphy, J.B., Evans, N.J., Xia, X.-P., 2022. Formation of juvenile continental crust in northern Nubian Shield: New evidence from granitic zircon U-Pb-Hf-O isotopes. Precambrian Res. 379,. https://doi.org/10.1016/j.precamres.2022.106791 106791.
Garzanti, E., Gaetani, M., 2002. Unroofing history of Late Paleozoic magmatic arcs within the "Turan Plate" (Tuarkyr, Turkmenistan). Sediment. Geol. 151 (1), 67–87. https://doi.org/10.1016/S0037-0738(01)00231-7.
Geyer, G., Bayet-Goll, A., Wilmsen, M., Mahboubi, A., Moussavi-Harami, R., 2014. Lithostratigraphic revision of the middle Cambrian (Series 3) and upper Cambrian (Furongian) in northern and central Iran. Newslett. Stratig. 47 (1), 21–59. https://doi.org/10.1127/0078-0421/2014/0039.
Gharibnejad, P., Agard, P., Rosenberg, C.L., Omrani, J., Kananian, A., 2020. Fossil thermal structure of the southern Sanandaj-Sirjan zone (SW Iran): Implications for regional-scale tectonics. J. Asian Earth Sci. 200,. https://doi.org/10.1016/j.jseaes.2020.104488 104488.
Ghavidel- Syooki, m. (2019). Middle-Late Cambrian acritarchs from the Zardkuh area in the High Zagros Mountains, southern Iran: Stratigraphic and paleogeographic implications. *J. Sci. I. R. Iran, 30*(4), 331-353. doi:10.22059/jsciences.2019.267184.1007333.
Ghavidel-syooki, M., 1994a. Palynological study and age determination of Ordovician sediments and Faraghan Formation in Kuh-e-Surmeh at southern Iran. J. Geosci. 3 (12), 28–35.
Ghavidel-syooki, M., 1994b. Upper Devonian acritarchs and miospores from the Geirud Formation in Central Alborz Range, northern Iran. J. Sci. i. r. Iran 5 (3), 103–122.
Ghavidel-syooki, M., 2006. Palynostratigraphy and palaeogeography of the Cambro-Ordovician strata in southwest of Shahrud City (Kuh-e-Kharbash, near Deh-Molla), Central Alborz Range, northern Iran. Rev. Palaeobot. Palynol. 139 (1), 81–95. https://doi.org/10.1016/j.revpalbo.2005.07.006.
Ghavidel-syooki, M., 2017. Biostratigraphy of Acritarchs and Chitinozoans in Ordovician Strata from the Fazel Abad Area, Southeastern Caspian Sea, Alborz Mountains, Northern Iran: Stratigraphic Implications. J. Sci. i. r. Iran 28 (1), 37–57.
Ghavidel-Syooki, M., 2021. Peri-Gondwanan acritarchs, chitinozoans, and miospores from Paleozoic succession in the High Zagros Mountains, southern Iran: Regional stratigraphic significance and paleogeographic implications. Rev. Palaeobot. Palynol. 292,. https://doi.org/10.1016/j.revpalbo.2021.104457 104457.
Ghavidel-Syooki, M., Hassanzadeh, J., Vecoli, M., 2011b. Palynology and isotope geochronology of the Upper Ordovician-Silurian successions (Ghelli and Soltan Maidan Formations) in the Khoshyeilagh area, eastern Alborz Range, northern Iran; stratigraphic and palaeogeographic implications. Rev. Palaeobot. Palynol. 164 (3–4), 251–271. https://doi.org/10.1016/j.revpalbo.2011.01.006.
Ghavidel-Syooki, M., Popov, L.E., Alvaro, J.J., Ghobadi Pour, M., Tolmacheva, T.Y., Ehsani, M.H., 2014. Dapingian-lower Darriwilian (Ordovician) stratigraphic gap in the Faraghan Mountains, Zagros Ranges, south-eastern Iran. Bull. Geosci. 89 (4), 679–706.
Ghavidel-syooki, M., Vecoli, M., 2008. Palynostratigraphy of Middle Cambrian to lowermost Ordovician stratal sequences in the High Zagros Mountains, southern Iran: Regional stratigraphic implications, and palaeobiogeographic significance. Rev. Palaeobot. Palynol. 150 (1), 97–114. https://doi.org/10.1016/j.revpalbo.2008.01.006.
Ghavidel-syooki, M., Álvaro, J.J., Popov, L., Pour, M.G., Ehsani, M.H., Suyarkova, A., 2011a. Stratigraphic evidence for the Hirnantian (latest Ordovician) glaciation in the Zagros Mountains. Iran*Palaeogeog. Palaeoclimatol. Palaeoecol.* 307 (1–4), 1–16. https://doi.org/10.1016/j.palaeo.2011.04.011.
Ghobadi Pour, M., 2019. Ordovician trilobites from Deh-Molla, eastern Alborz. Iran*Alhceringa: Aust. J. Palaeontol.* 43 (3), 381–405. https://doi.org/10.1080/03115518.2019.1616110.
Ghobadi Pour, M., Kebriaee-Zadeh, M., Popov, L., 2011. Early Ordovician (Tremadocian) Brachiopods from the Eastern Alborz Mountains. Iran*Est. J. Earth Sci.* 60 (2), 65–82. https://doi.org/10.3176/earth.2011.2.01.
Ghobadi Pour, M., Ghavidel-Syooki, M., Álvaro, J.J., Popov, L.E., Ehsani, M.H., 2015. First reported Late Ordovician trilobites from the High Zagros Ranges, Iran: A biogeographic link between Gondwanan Chinese and Mediterranean faunas. Geobios 48 (5), 351–369. https://doi.org/10.1016/j.geobios.2015.07.005.
Ghobadi Pour, M., Popov, L., 2009. First Report on the Occurrence of Neseuretinus and Ovalocephalus Trilobites in the Middle Ordovician of Iran. Acta Palaeontol. Polon. 125–133. https://doi.org/10.4202/app.2009.0113.
Ghobadi Pour, M., Williams, M., Vannier, J., Meidla, T., Popov, L., 2006. Ordovician ostracods from east central Iran. Acta Palaeontol. Polon. 51 (3), 551–560.
Gholami Zadeh, P., Adabi, M.H., Ghassemi, M.R., Sadeghi, A., Eshraghi, S.A., 2020. Mélange development in the Neyriz region of Zagros Orogen, Iran: Record of convergence and collision in the Neotethyan Realm. Basin Res. 32 (6), 1626–1652. https://doi.org/10.1111/bre.12445.
Gholami Zadeh, P., Hu, X., Garzanti, E., Adabi, M.H., 2021. Constraining the timing of Arabia-Eurasia collision in the Zagros orogen by sandstone provenance (Neyriz, Iran). Geol. Soc. Am. Bull. 134 (7–8), 1793–1810. https://doi.org/10.1130/B35950.1.
Gholipour, S., Azizi, H., Masoudi, F., Asahara, Y., Minami, M., 2022. S-type like granites and felsic volcanic rocks in the Mahabad area, NW Iran: Late Neoproterozoic extensional tectonics follow collision on the northern boundary of Gondwana. Lithos 416–417,. https://doi.org/10.1016/j.lithos.2022.106658 106658.
Ghorbani, M., 2019. Lithostratigraphy of Iran. Springer Geology, Springer, Cham.
Golestani, M., 2020. Characteristics of tectono-magmatic alkali gabbros in northern Fathabad, Zarand (NW Kerman): based on the pyroxene mineral chemistry. [ویژگی های تکتونو-ماگمایی گابروهای قلیایی در شمال فتح آباد زرند (شمال غرب کرمان): بر پایه ی شیمی کانی پیروکسن]. Iran. J. Crystallogr. Mineral. 28 (2), 311–328. https://doi.org/10.29252/ijcm.28.2.311.
Gyomlai, T., Agard, P., Jolivet, L., Larvet, T., Bonnet, G., Omrani, J., Larson, K., Caron, B., Noël, J., 2022. Cimmerian metamorphism and post Mid-Cimmerian exhumation in Central Iran: Insights from in-situ Rb/Sr and U/Pb dating. J. Asian Earth Sci. 233,. https://doi.org/10.1016/j.jseaes.2022.105242 105242.
Hairapetian, V., Ghobadi Pour, M., Popov, L., Hejazi, S., Holmer, L., Evans, D., & Sharafi, A. (2015). Ordovician of the Anarak Region: implications in understanding Early Palaeozoic history of Central Iran. *Stratigraphy, Supplement to volume 12*(2), 22-29.
Hargrove, U.S., Stern, B., Griffin, W., Johnson, P., Abdelsalam, M., 2006a. From Island Arc to Craton: Timescales of Crustal Formation along the Neoproterozoic Bi'r Umq Suture zone. Retrieved from, Kingdom of Saudi Arabia.
Hargrove, U.S., Stern, R.J., Kimura, J.I., Manton, W.I., Johnson, P.R., 2006b. How juvenile is the Arabian-Nubian Shield? Evidence from Nd isotopes and pre-Neoproterozoic inherited zircon in the Bi'r Umq suture zone. Saudi Arabia. *Earth Planet. Sci. Lett.* 252 (3), 308–326. https://doi.org/10.1016/j.epsl.2006.10.002.
Hargrove, U. S., I.,II. . (2006). *Crustal evolution of the neoproterozoic bi'r umq suture zone, kingdom of saudi arabia: Geochronological, isotopic, and* geochemical *constraints.* (PhD Thesis), United States, Texas. Retrieved from https://search-proquest-com.ezproxy.lib.monash.edu.au/docview/304953080?accountid=12528 (3225070).
Hassan, M., Stüwe, K., Abu-Alam, T.S., Klötzli, U., Tiepolo, M., 2016. Time constraints on deformation of the Ajjaj branch of one of the largest Proterozoic shear zones on Earth: The Najd Fault System. Gondwana Res. 34, 346–362. https://doi.org/10.1016/j.gr.2015.04.009.
Hassanzadeh, J., Wernicke, B.P., 2016. The Neotethyan Sanandaj-Sirjan zone of Iran as an archetype for passive margin-arc transitions. Tectonics 35 (3), 586–621. https://doi.org/10.1002/2015TC003926.
Hassanzadeh, J., Stockli, D.F., Horton, B.K., Axen, G.J., Stockli, L.D., Grove, M., Schmitt, A.K., Walker, J.D., 2008. U-Pb zircon geochronology of late Neoproterozoic-Early Cambrian granitoids in Iran: Implications for paleogeography, magmatism, and exhumation history of Iranian basement. Tectonophysics 451 (1), 71–96. https://doi.org/10.1016/j.tecto.2007.11.062.
Honarmand, M., Li, X.-H., Nabatian, G., Rezaeian, M., Etemad-Saeed, N., 2016. Neoproterozoic-Early Cambrian tectono-magmatic evolution of the Central Iranian terrane, northern margin of Gondwana: Constraints from detrital zircon U-Pb and Hf–O isotope studies. Gondwana Res. 37, 285–300. https://doi.org/10.1016/j.gr.2016.05.007.
Honarmand, M., Xiao, W., Nabatian, G., Blades, M.L., dos Santos, M.C., Collins, A.S., Ao, S., 2018. Zircon U-Pb-Hf isotopes, bulk-rock geochemistry and Sr-Nd-Pb isotopes from late Neoproterozoic basement in the Mahneshan area, NW Iran: Implications for Ediacaran active continental margin along the northern Gondwana and constraints on the late Oligocene crustal anatexis. Gondwana Res. 57, 48–76. https://doi.org/10.1016/j.gr.2017.12.009.
Horton, B.K., Hassanzadeh, J., Stockli, D.F., Axen, G.J., Gillis, R.J., Guest, B., Amini, A., Fakhari, M.D., Zamanzadeh, S.M., Grove, M., 2008. Detrital zircon provenance of Neoproterozoic to Cenozoic deposits in Iran: Implications for chronostratigraphy and collisional tectonics. Tectonophysics 451 (1), 97–122. https://doi.org/10.1016/j.tecto.2007.11.063.
Jamei, S., Ghorbani, M., Williams, I.S., Moayyed, M., 2020. Tethyan oceans reconstructions with emphasis on the Early Carboniferous Pir-Eshagh A-type rhyolite and the Late Palaeozoic magmatism in Iran. Int. Geol. Rev. 1–17. https://doi.org/10.1080/00206814.2020.1768443.
Jamei, S., Ghorbani, M., Jafari, A., Williams, I.S., Moayyed, M., 2021. Geochronology and tectonic significance of A-type granite from Misho, NW Iran: Implications for the detachment of Cimmeria from Gondwana and the opening of Neo-Tethys. Geol. J. 56 (10), 5275–5289. https://doi.org/10.1002/gj.4236.
Jazimagh, N., Bayet-Goll, A., & Sharafi, M. (2020). *Provenance and petrography of early to middle Ordovician samdstone sof Lashkarak Formation, Central alborz, Irann.* Paper presented at the 39 National Congress and 4th International Congress of Earth Sciences, Tehran, Iran. https://civilica.com/doc/1202463.
Johnson, P.R., Andresen, A., Collins, A.S., Fowler, A.R., Fritz, H., Ghebreab, W., Kusky, T., Stern, R.J., 2011. Late Cryogenian-Ediacaran history of the Arabian-Nubian

Shield: A review of depositional, plutonic, structural, and tectonic events in the closing stages of the northern East African Orogen. J. Afr. Earth Sci. 61 (3), 167–232. https://doi.org/10.1016/j.jafrearsci.2011.07.003.
Johnson, P. R., Kattan, F. H., & Al-Saleh, A. M. (2004). Neoproterozoic Ophiolites in the Arabian Shield: Field Relations and Structure. In *Developments in Precambrian Geology* (Vol. 13, pp. 129-162): Elsevier.
Johnson, P.R., Woldehaimanot, B., 2003. Development of the Arabian-Nubian Shield: perspectives on accretion and deformation in the northern East African Orogen and the assembly of Gondwana. Geol. Soc. Spec. Pub. 206 (1), 289. https://doi.org/10.1144/GSL.SP.2003.206.01.15.
Kargaranbafghi, F., Neubauer, F., Genser, J., Faghih, A., Kusky, T., 2012. Mesozoic to Eocene ductile deformation of western Central Iran: From Cimmerian collisional orogeny to Eocene exhumation. Tectonophysics 564–565, 83–100. https://doi.org/10.1016/j.tecto.2012.06.017.
Karimpour, M.H., Stern, C.R., Farmer, G.L., 2010. Zircon U-Pb geochronology, Sr–Nd isotope analyses, and petrogenetic study of the Dehnow diorite and Kuhsangi granodiorite (Paleo-Tethys). NE Iran. *J. Asian Earth Sci.* 37 (4), 384–393. https://doi.org/10.1016/j.jseaes.2009.11.001.
Kebria-ee Zadeh, M.-R., Ghobadi Pour, M., Popov, L., Baars, C., Jahangir, H., 2015. First record of the Ordovician fauna in Mila-Kuh, eastern Alborz, northern Iran. Est. J. Earth Sci. 64 (2). https://doi.org/10.3176/earth.2015.22.
Khalatbari Jafari, M., Babaie, H.A., Gani, M., 2013. Geochemical evidence for Late Cretaceous marginal arc-to-backarc transition in the Sabzevar ophiolitic extrusive sequence, northeast Iran. J. Asian Earth Sci. 70–71, 209–230. https://doi.org/10.1016/j.jseaes.2013.03.015.
Khalili, K., Torabi, G., Arai, S., 2016. Metamorphism of peridotites from Posht-e-Badam Paleozoic ophiolite (Yazd Province, Central Iran). Neues Jahrb. Geol. Palaontol. Abhand. 280 (1), 59–77. https://doi.org/10.1127/njgpa/2016/0565.
Khazaei, E., Mahmoudy-Gharaie, M.H., Mahboubi, A., Moussavi-Harami, R., Taheri, J., 2018. Petrography, Major and Trace Elemental Geochemistry of the Ordovician-Silurian Siliciclastics in North of Tabas Block, Central Iran: Implications for Provenance and Paleogeography. J. Sci. i. r. Iran 29 (2), 129–142. https://doi.org/10.22059/jsciences.2018.65019.
Koshnaw, R.I., Schlunegger, F., Stockli, D.F., 2021. Detrital zircon provenance record of the Zagros mountain building from the Neotethys obduction to the Arabia-Eurasia collision, NW Zagros fold–thrust belt. Kurdistan Region of Iraq. *Solid Earth* 12 (11), 2479–2501. https://doi.org/10.5194/se-12-2479-2021.
Kozdrój, W., Kennedy, A.K., Johnson, P.R., Ziółkowska-Kozdrój, M., Kadi, K., 2018. Geochronology in the southern Midyan terrane: a review of constraints on the timing of magmatic pulses and tectonic evolution in a northwestern part of the Arabian Shield. Int. Geol. Rev. 60 (10), 1290–1319. https://doi.org/10.1080/00206814.2017.1385425.
Kröner, A., Sassi, F.P., 1996. Evolution of the northern Somali basement: new constraints from zircon ages. J. Afr. Earth Sci. 22 (1), 1–15. https://doi.org/10.1016/0899-5362(95)00121-2.
Li, X.-H., Abd El-Rahman, Y., Abu Anbar, M., Li, J., Ling, X.-X., Wu, L.-G., Masoud, A.E., 2018. Old Continental Crust Underlying Juvenile Oceanic Arc: Evidence From Northern Arabian-Nubian Shield. Egypt. *Geophys. Res. Lett.* 45 (7), 3001–3008. https://doi.org/10.1002/2018GL077121.
Luvizotto, G.L., Zack, T., 2009. Nb and Zr behavior in rutile during high-grade metamorphism and retrogression: An example from the Ivrea-Verbano Zone. Chem. Geol. 261 (3), 303–317. https://doi.org/10.1016/j.chemgeo.2008.07.023.
Mahmudy Gharaie, M. H., Matsumoto, R., Kakuwa, Y., & Milroy, P. (2004). Late Devonian facies variety in Iran: Volcanism as a possible *trigger* of the environmental perturbation near the Frasnian-Famennian boundary. *Geol. Q., 48*, 323-332. doi:https://gq.pgi.gov.pl/article/view/7356.
Masoodi, M., Yassaghi, A., Nogole Sadat, M.A.A., Neubauer, F., Bernroider, M., Friedl, G., Genser, J., Houshmandzadeh, A., 2013. Cimmerian evolution of the Central Iranian basement: Evidence from metamorphic units of the Kashmar-Kerman Tectonic Zone. Tectonophysics 588, 189–208. https://doi.org/10.1016/j.tecto.2012.12.012.
Masri, A., 2017. Late Ordovician glacial and glacio-fluvial paleovalley architecture and sedimentation in southeast Jordan and northwest Saudi Arabia. Arab. J. Geosci. 10 (13), 288. https://doi.org/10.1007/s12517-017-3081-2.
Mattei, M., Cifelli, F., Muttoni, G., Zanchi, A., Berra, F., Mossavvari, F., Eshraghi, S.A., 2012. Neogene block rotation in central Iran: Evidence from paleomagnetic data. Geol. Soc. Am. Bull. 124 (5–6), 943–956. https://doi.org/10.1130/B30479.1.
Mattei, M., Cifelli, F., Muttoni, G., Rashid, H., 2015. Post-Cimmerian (Jurassic–Cenozoic) paleogeography and vertical axis tectonic rotations of Central Iran and the Alborz Mountains. J. Asian Earth Sci. 102, 92–101. https://doi.org/10.1016/j.jseaes.2014.09.038.
Matthews, W.A., Guest, B., 2017. A Practical Approach for Collecting Large-n Detrital Zircon U-Pb Data sets by Quadrupole LA-ICP-MS. Geostand. Geoanal. Res. 41 (2), 161–180. https://doi.org/10.1111/ggr.12146.
Mehdipour Ghazi, J., Moazzen, M., Rahgoshay, M., Wilde, S.A., 2020. Zircon U-Pb–Hf isotopes and whole rock geochemistry of magmatic rocks from the Posht-e-Badam Block: A key to tectonomagmatic evolution of Central Iran. Gondwana Res. 87, 162–187. https://doi.org/10.1016/j.gr.2020.06.010.
Mehdizadeh Shahri, H. (2008). Pre-rifting Evidence of Paleotethys in the Southwest of Shahrood, Northeastern Iran. *World Appl. Sci. J., 3*(1), 154-161. doi:https://idosi.org/wasj/wasj3(1)/26.pdf.
Metcalfe, I., 2021. Multiple Tethyan ocean basins and orogenic belts in Asia. Gondwana Res. 100, 87–130. https://doi.org/10.1016/j.gr.2021.01.012.
Moghadam, H.S., Li, X.-H., Griffin, W.L., Stern, R.J., Thomsen, T.B., Meinhold, G., Aharipour, R., O'Reilly, S.Y., 2017a. Early Paleozoic tectonic reconstruction of Iran: Tales from detrital zircon geochronology. Lithos 268–271, 87–101. https://doi.org/10.1016/j.lithos.2016.09.008.
Moghadam, H.S., Li, X.-H., Santos, J.F., Stern, R.J., Griffin, W.L., Ghorbani, G., Sarebani, N., 2017b. Neoproterozoic magmatic flare-up along the N. margin of Gondwana: The Taknar complex. NE Iran. *Earth Planet. Sci. Lett.* 474, 83–96. https://doi.org/10.1016/j.epsl.2017.06.028.
Moghadam, H.S., Li, Q.L., Griffin, W.L., Stern, R.J., Santos, J.F., Lucci, F., Beyarslan, M., Ghorbani, G., Ravankhah, A., Tilhac, R., O'Reilly, S.Y., 2021. Prolonged magmatism and growth of the Iran-Anatolia Cadomian continental arc segment in Northern Gondwana. Lithos 384–385,. https://doi.org/10.1016/j.lithos.2020.105940 105940.
Moghadam, H.S., Stern, R.J., 2015. Ophiolites of Iran: Keys to understanding the tectonic evolution of SW Asia: (II) Mesozoic ophiolites. J. Asian Earth Sci. 100, 31–59. https://doi.org/10.1016/j.jseaes.2014.12.016.
Moghadam, H.S., Li, X.H., Stern, R.J., Santos, J.F., Ghorbani, G., Pourmohsen, M., 2016. Age and nature of 560–520 Ma calc-alkaline granitoids of Biarjmand, northeast Iran: insights into Cadomian arc magmatism in northern Gondwana. Int. Geol. Rev. 58 (12), 1492–1509. https://doi.org/10.1080/00206814.2016.1166461.
Moghadam, H.S., Stern, R.J., Griffin, W.L., Khedr, M.Z., Kirchenbaur, M., Ottley, C.J., Whattam, S.A., Kimura, J.I., Ghorbani, G., Gain, S., O'Reilly, S.Y., Tamura, A., 2019. Subduction initiation and back-arc opening north of Neo-Tethys: Evidence from the Late Cretaceous Torbat-e-Heydarieh ophiolite of NE Iran. Geol. Soc. Am. Bull. 132 (5–6), 1083–1105. https://doi.org/10.1130/B35065.1.
Mohammadi, A., Moazzen, M., Lechmann, A., Laurent, O., 2020. Zircon U-Pb geochronology and geochemistry of Late Devonian-Carboniferous granitoids in NW Iran: implications for the opening of Paleo-Tethys. Int. Geol. Rev. 62 (15), 1931–1948. https://doi.org/10.1080/00206814.2019.1675540.
Monsef, R., Monsef, I., Rahgoshay, M., 2014. GEODYNAMIC SIGNIFICANCE OF THE JANATABAD PERIDOTITES AND ASSOCIATED CHROMITITES (S IRAN): IMPLICATIONS FOR SUBDUCTION INITIATION. Ofioliti 39 (2), 67–78. https://doi.org/10.4454/ofioliti.v39i2.430.
Monsef, I., Monsef, R., Mata, J., Zhang, Z., Pirouz, M., Rezaeian, M., Esmaeili, R., Xiao, W., 2018a. Evidence for an early-MORB to fore-arc evolution within the Zagros suture zone: Constraints from zircon U-Pb geochronology and geochemistry of the Neyriz ophiolite (South Iran). Gondwana Res. 62, 287–305. https://doi.org/10.1016/j.gr.2018.03.002.
Monsef, I., Rahgoshay, M., Pirouz, M., Chiaradia, M., Grégoire, M., Ceuleneer, G., 2018b. The Eastern Makran Ophiolite (SE Iran): evidence for a Late Cretaceous fore-arc oceanic crust. Int. Geol. Rev. 1–27. https://doi.org/10.1080/00206814.2018.1507764.
Monsef, I., Zhang, Z., Shabanian, E., le Roux, P., Rahgoshay, M., 2022. Tethyan subduction and Cretaceous rift magmatism at the southern margin of Eurasia: Evidence for crustal evolution of the South Caspian Basin. Earth-Sci. Rev. 228,. https://doi.org/10.1016/j.earscirev.2022.104012 104012.
Moradi, A., Shabanian, N., Davoudian, A.R., Azizi, H., Santos, J.F., Asahara, Y., 2022. Geochronology and petrogenesis of the Late Neoproterozoic granitic gneisses of Golpayegan metamorphic complex: a new respect for Cadomian crust in the Sanandaj-Sirjan zone. Iran*Int. Geol. Rev.* 64 (10), 1450–1473. https://doi.org/10.1080/00206814.2020.1821251.
Morag, N., Avigad, D., Gerdes, A., Belousova, E., Harlavan, Y., 2011. Crustal evolution and recycling in the northern Arabian-Nubian Shield: New perspectives from zircon Lu–Hf and U-Pb systematics. Precambrian Res. 186 (1), 101–116. https://doi.org/10.1016/j.precamres.2011.01.004.
Mulder, J.A., Nebel, O., Gardiner, N.J., Cawood, P.A., Wainwright, A.N., Ivanic, T.J., 2021. Crustal rejuvenation stabilised Earth's first cratons. Nat. Commun. 12 (1), 3535. https://doi.org/10.1038/s41467-021-23805-6.
Muttoni, G., Gaetani, M., Kent, D.V., Sciunnach, D., Angiolini, L., Berra, F., Garzanti, E., Mattei, M., Zanchi, A., 2009a. Opening of the Neo-Tethys Ocean and the Pangea B to Pangea A transformation during the Permian. Geoarabia 14 (4), 17–48. https://doi.org/10.2113/geoarabia140417.
Muttoni, G., Mattei, M., Balini, M., Zanchi, A., Gaetani, M., Berra, F., 2009b. The drift history of Iran from the Ordovician to the Triassic. Geol. Soc. Spec. Pub. 312 (1), 7–29. https://doi.org/10.1144/SP312.2.
Nance, R.D., Gutiérrez-Alonso, G., Keppie, J.D., Linnemann, U., Murphy, J.B., Quesada, C., Strachan, R.A., Woodcock, N.H., 2010. Evolution of the Rheic Ocean. Gondwana Res. 17 (2), 194–222. https://doi.org/10.1016/j.gr.2009.08.001.
Nasiri Bezenjani, R., Pease, V., Whitehouse, M.J., Shalaby, M.H., Kadi, K.A., Kozdroj, W., 2014. Detrital zircon geochronology and provenance of the Neoproterozoic Hammamat Group (Igla Basin), Egypt and the Thalbah Group, NW Saudi Arabia: Implications for regional collision tectonics. Precambrian Res. 245, 225–243. https://doi.org/10.1016/j.precamres.2013.12.002.
Natal'in, B.A., Şengör, A.M.C., 2005. Late Palaeozoic to Triassic evolution of the Turan and Scythian platforms: The pre-history of the Palaeo-Tethyan closure. Tectonophysics 404 (3), 175–202. https://doi.org/10.1016/j.tecto.2005.04.011.
Nouri, F., Reza Davoudian, A., Allen, M.B., Azizi, H., Asahara, Y., Anma, R., Shabanian, N., Tsuboi, M., Khodami, M., 2021. Early Cambrian highly fractionated granite, Central Iran: Evidence for drifting of northern Gondwana and the evolution of the Proto-Tethys Ocean. Precambrian Res. 362,. https://doi.org/10.1016/j.precamres.2021.106291 106291.
Nouri, F., Davoudian, A.R., Shabanian, N., Allen, M.B., Asahara, Y., Azizi, H., Anma, R., Khodami, M., Tsuboi, M., 2022. Tectonic transition from Ediacaran continental arc to early Cambrian rift in the NE Ardakan region, central Iran: Constraints from geochronology and geochemistry of magmatic rocks. J. Asian Earth Sci. 224,. https://doi.org/10.1016/j.jseaes.2021.105011 105011.
Nutman, A.P., Mohajjel, M., Bennett, V.C., Fergusson, C.L., 2013. Gondwanan Eoarchean-Neoproterozoic ancient crustal material in Iran and Turkey: zircon

U-Pb–Hf isotopic evidence. Can. J. Earth Sci. 51 (3), 272–285. https://doi.org/10.1139/cjes-2013-0138.
Paton, C., Hellstrom, J., Paul, B., Woodhead, J., Hergt, J., 2011. Iolite: Freeware for the visualisation and processing of mass spectrometric data. J. Anal. at. Spectrom. 26 (12), 2508–2518. https://doi.org/10.1039/C1JA10172B.
Pease, V., Yeshanew, F.G., Whitehouse, M.J., 2022. Deciphering crustal growth in the southernmost Arabian Shield through zircon U-Pb geochronology, whole rock chemistry and Nd isotopes. Int. Geol. Rev. 64 (16), 2359–2377. https://doi.org/10.1080/00206814.2021.1983735.
Pirnia, T., Saccani, E., Torabi, G., Chiari, M., Goričan, Š., Barbero, E., 2020. Cretaceous tectonic evolution of the Neo-Tethys in Central Iran: Evidence from petrology and age of the Nain-Ashin ophiolitic basalts. Geosci. Front. 11 (1), 57–81. https://doi.org/10.1016/j.gsf.2019.02.008.
Popov, L.E., Vachik, H., Evans, D.H., Mansoureh Ghobadi, P., Holmer, L.E., Baars, C., 2015. Review of the Ordovician stratigraphy and fauna of the Anarak Region in Central Iran. Acta Geol. Polon. 65 (4), 403–435. https://doi.org/10.1515/agp-2015-0019.
Rahimi-Chakdel, A., Raghimi, M., 2014. Some characteristics of mafic dykes in Gondwanan land from South of Gorgan, Northeastern Iran: Implication to Petrogenesis and Paleotectonic. Q. J. Tethys 2 (2), 137–147.
Rahmati-Ilkhchi, M., Jeřábek, P., Faryad, S.W., Koyi, H.A., 2010. Mid-Cimmerian, Early Alpine and Late Cenozoic orogenic events in the Shotur Kuh metamorphic complex, Great Kavir block. NE Iran. *Tectonophysics* 494 (1), 101–117. https://doi.org/10.1016/j.tecto.2010.09.005.
Ramezani, J., Tucker, R.D., 2003. The Saghand Region, Central Iran: U-Pb geochronology, petrogenesis and implications for Gondwana Tectonics. Am. J. Sci. 303 (7), 622–665. https://doi.org/10.2475/ajs.303.7.622.
Ranjbar Moghadam, F., Masoudi, F., Corfu, F., Homam, S.M., 2018. Ordovician mafic magmatism in an Ediacaran arc complex, Sibak, northeastern Iran: the eastern tip of the Rheic Ocean. Can. J. Earth Sci. 55 (10), 1173–1182. https://doi.org/10.1139/cjes-2018-0072.
Robertson, A.H.F., Parlak, O., Ustaömer, T., 2021. Late Palaeozoic extensional volcanism along the northern margin of Gondwana in southern Turkey: implications for Palaeotethyan development. Int. J. Earth Sci. 110 (6), 1961–1994. https://doi.org/10.1007/s00531-021-02051-7.
Robinson, F.A., Foden, J.D., Collins, A.S., Payne, J.L., 2014. Arabian Shield magmatic cycles and their relationship with Gondwana assembly: Insights from zircon U-Pb and Hf isotopes. Earth Planet. Sci. Lett. 408, 207–225. https://doi.org/10.1016/j.epsl.2014.10.010.
Robinson, F.A., Foden, J.D., Collins, A.S., 2015. Geochemical and isotopic constraints on island arc, synorogenic, post-orogenic and anorogenic granitoids in the Arabian Shield, Saudi Arabia. Lithos 220–223, 97–115. https://doi.org/10.1016/j.lithos.2015.01.021.
Robinson, F.A., Pease, V., Whitehouse, M.J., Kooijman, E., 2018. Preliminary detrital zircon signatures from the southern Asir terrane, Saudi Arabia: A link to Yemen or the Nubian Shield? Precambrian Res. 311, 247–261. https://doi.org/10.1016/j.precamres.2018.04.017.
Rossetti, F., Nozaem, R., Lucci, F., Vignaroli, G., Gerdes, A., Nasrabadi, M., Theye, T., 2015. Tectonic setting and geochronology of the Cadomian (Ediacaran-Cambrian) magmatism in Central Iran, Kuh-e-Sarhangi region (NW Lut Block). J. Asian Earth Sci. 102, 24–44. https://doi.org/10.1016/j.jseaes.2014.07.034.
Ruttner, A., Nabavi, M., & Hajian, J. (1968). *Geology of the Shirgesht area (Tabas area, East Iran)*. Iran: Geological Society of Iran, Report 4.
Saccani, E., Azimzadeh, Z., Dilek, Y., Jahangiri, A., 2013. Geochronology and petrology of the Early Carboniferous Misho Mafic Complex (NW Iran), and implications for the melt evolution of Paleo-Tethyan rifting in Western Cimmeria. Lithos 162–163, 264–278. https://doi.org/10.1016/j.lithos.2013.01.008.
Salerno, V.M., Capitanio, F.A., Farrington, R.J., Riel, N., 2016. The role of long-term rifting history on modes of continental lithosphere extension. J. Geophys. Res. Solid Earth 121 (12), 8917–8940. https://doi.org/10.1002/2016JB013005.
Samadi, R., Torabi, G., Dantas, E.L., Morishita, T., Kawabata, H., 2022. Ordovician crustal thickening and syn-collisional magmatism of Iran: Gondwanan basement along the north of the Yazd Block (Central Iran). Int. Geol. Rev. 64 (15), 2151–2165. https://doi.org/10.1080/00206814.2021.1972352.
Schallreuter, R., Hinz-Schallreuter, I., Balini, M., Ferretti, A., 2006. Late Ordovician Ostracoda from Iran and their significance for Palaeogeographic reconstructions. Z. Geol. Wiss. 34 (5), 293–345.
Sciuba, M., Beaudoin, G., 2021. Texture and Trace Element Composition of Rutile in Orogenic Gold Deposits. Econ. Geol. 116 (8), 1865–1892. https://doi.org/10.5382/econgeo.4857.
Sepidbar, F., Moghadam, H.S., Li, C., Stern, R.J., Jiantang, P., Vesali, Y., 2020. Cadomian Magmatic Rocks from Zarand (SE Iran) Formed in a Retro-Arc Basin. Lithos 366–367,. https://doi.org/10.1016/j.lithos.2020.105569 105569.
Sepidbar, F., Ghorbani, G., Zoheir, B., Palin, R.M., Homam, S.M., Zafar, T., Ma, J., He, L., 2021. Coeval calc-alkaline and alkaline Cadomian magmatism in the Bafq, central Iran: Insights into their petrogenesis. Lithos 406–407,. https://doi.org/10.1016/j.lithos.2021.106535 106535.
Sepidbar, F., Homam, S.M., Wu, G., Moritz, R., Hafezimoghadas, H., 2023. Early Paleozoic mafic intraplate magmatism in the Binaloud zone, NE Iran: Implications for the long-lived mantle plume activity in the northern margin of Gondwana. Lithos 450–451,. https://doi.org/10.1016/j.lithos.2023.107191 107191.
Shafaii Moghadam, H., Griffin, W.L., Li, X.-H., Santos, J.F., Karsli, O., Stern, R.J., Ghorbani, G., Gain, S., Murphy, R., O'Reilly, S.Y., 2017. Crustal Evolution of NW Iran: Cadomian Arcs, Archean Fragments and the Cenozoic Magmatic Flare-Up. J. Petrol. 58 (11), 2143–2190. https://doi.org/10.1093/petrology/egy005.
Shafaii Moghadam, H., Li, Q.L., Griffin, W.L., Stern, R.J., Ishizuka, O., Henry, H., Lucci, F., O'Reilly, S.Y., Ghorbani, G., 2020a. Repeated magmatic buildup and deep "hot zones" in continental evolution: The Cadomian crust of Iran. Earth Planet. Sci. Lett. 531,. https://doi.org/10.1016/j.epsl.2019.115989 115989.
Shafaii Moghadam, H., Li, Q.L., Li, X.H., Stern, R.J., Levresse, G., Santos, J.F., Lopez Martinez, M., Ducea, M.N., Ghorbani, G., Hassannezhad, A., 2020b. Neotethyan Subduction Ignited the Iran Arc and Backarc Differently. J. Geophys. Res. Solid Earth 125 (5). https://doi.org/10.1029/2019JB018460.
Shafaii Moghadam, H., Stern, R.J., 2014. Ophiolites of Iran: Keys to understanding the tectonic evolution of SW Asia: (I) Paleozoic ophiolites. J. Asian Earth Sci. 91, 19–38. https://doi.org/10.1016/j.jseaes.2014.04.008.
Shahsavari Alavijeh, B., Rashidnejad-Omran, N., Toksoy-Köksal, F., Chew, D., Szopa, K., Ghalamghash, J., Gaweda, A., 2019. Geochemistry and apatite U-Pb geochronology of alkaline gabbros from the Nodoushan plutonic complex, Sanandaj-Sirjan Zone, Central Iran: Evidence for Early Palaeozoic rifting of northern Gondwana. Geol. J. 54 (4), 1902–1926. https://doi.org/10.1002/gj.3270.
Shakerardakani, F., Neubauer, F., Liu, X., Dong, Y., Monfaredi, B., Li, X.-H., 2021. New detrital zircon U-Pb insights on the palaeogeographic origin of the central Sanandaj-Sirjan zone. Iran*Geol. Mag.* 158 (12), 2165–2186. https://doi.org/10.1017/S0016756821000728.
Sharland, P., Archer, R., M. Casey, D., Davies, R., Hall, S. H., Heward, A., D. Horbury, A., & Simmons, M. (2001). *Arabian Plate Sequence Stratigraphy* Gulf PetoLink, Bahrain: GeoArabia, Special Publication 2.
Sheikholeslami, M. R. (2017). Tectono-stratigraphic evidence for the opening and closure of the Neotethys Ocean in the southern Sanandaj-Sirjan zone, Iran. In *Tectonic Evolution, Collision, and Seismicity of Southwest Asia: In Honor of Manuel Berberian's Forty-Five Years of Research Contributions* (Vol. 525, pp. 0). Retrieved from https://doi.org/10.1130/2016.2525(09) doi:10.1130/2016.2525(09).
Shirdashtzadeh, N., Torabi, G., Schaefer, B., 2018. A magmatic record of Neoproterozoic to Paleozoic convergence between Gondwana and Laurasia in the northwest margin of the Central-East Iranian Microcontinent. J. Asian Earth Sci. 166, 35–47. https://doi.org/10.1016/j.jseaes.2018.07.008.
Soffel, H.C., Rster, H.G., 1980. Apparent Polar Wander Path of Central Iran and its Geotectonic Interpretation. J. Geomagn. Geoelectr. 32 (Supplement3). https://doi.org/10.5636/jgg.32.Supplement3_SIII117.
Soffel, H.C., Schmidt, S., Davoudzadeh, M., Rolf, C., 1996. New palaeomagnetic data from Central Iran and a Triassic palaeoreconstruction. Geol. Rundsch. 85 (2), 293–302. https://doi.org/10.1007/BF02422235.
Spina, A., Cirilli, S., Ghorbani, M., Rettori, R., Sorci, A., Servais, T., 2020a. Middle-late Cambrian acritarchs of the Zagros Basin, southwestern Iran. Palynology 1–25. https://doi.org/10.1080/01916122.2020.1771624.
Spina, A., Cirilli, S., Sorci, A., Clayton, G., Gennari, V., Ghorbani, M., Ghorbani, M., Ovissi, M., Rettori, G., Rettori, R., 2020b. Palynology of the Permian succession from the Ajabshir area (Azerbaijan, Central Iran): a preliminary report. Geopersia 10 (1), 211–225. https://doi.org/10.22059/geope.2020.298640.648534.
Stacey, J.S., Kramers, J.D., 1975. Approximation of terrestrial lead isotope evolution by a two-stage model. Earth Planet. Sci. Lett. 26 (2), 207–221. https://doi.org/10.1016/0012-821X(75)90088-6.
Stampfli, G.M., Borel, G.D., 2002. A plate tectonic model for the Paleozoic and Mesozoic constrained by dynamic plate boundaries and restored synthetic oceanic isochrons. Earth Planet. Sci. Lett. 196 (1), 17–33. https://doi.org/10.1016/S0012-821X(01)00588-X.
Stampfli, G., Marcoux, J., Baud, A., 1991. Tethyan margins in space and time. Palaeogeog. Palaeoclimatol. Palaeoecol. 87 (1), 373–409. https://doi.org/10.1016/0031-0182(91)90142-E.
Stern, R.J., Ali, K.A., Abdelsalam, M.G., Wilde, S.A., Zhou, Q., 2012. U-Pb zircon geochronology of the eastern part of the Southern Ethiopian Shield. Precambrian Res. 206–207, 159–167. https://doi.org/10.1016/j.precamres.2012.02.008.
Stöcklin, J., 1968. Structural History and Tectonics of Iran1: A Review. AAPG Bull. 52 (7), 1229–1258. https://doi.org/10.1306/5D25C4A5-16C1-11D7-8645000102C1865D.
Stöcklin, J., 1974. Possible Ancient Continental Margins in Iran. In: Burk, C.A., Drake, C.L. (Eds.), The Geology of Continental Margins. Springer, Berlin Heidelberg, Berlin, Heidelberg, pp. 873–887.
Sultan, M., Tucker, R.D., El Alfy, Z., Attia, R., Ragab, A.G., 1994. U-Pb (zircon) ages for the gneissic terrane west of the Nile, southern Egypt. Geol. Rundsch. 83 (3), 514–522. https://doi.org/10.1007/BF00194158.
Teklay, M., Kröner, A., Mezger, K., & Oberhänsli, R. (1998). Geochemistry, PbPb single zircon ages and NdSr isotope composition of Precambrian rocks from southern and eastern Ethiopia: implications for crustal evolution in East Africa. *J. Afr. Earth Sci., 26*(2), 207-227. 10.1016/*S0899*-5362(98)00006-2.
Tomkins, H.S., Powell, R., Ellis, D.J., 2007. The pressure dependence of the zirconium-in-rutile thermometer. J. Metamorph. Geol. 25 (6), 703–713. https://doi.org/10.1111/j.1525-1314.2007.00724.x.
Torabi, G., Hashemi, F., 2010. Petrology of Devonian basalts from Pol-e-Khavand area (SE of Anarak, NE of Isfahan). Petrolog. J. 1 (3), 29–46.
Torsvik, T.H., Cocks, L.R.M., 2017. Earth History and Palaeogeography. Cambridge University Press, Cambridge.
Triebold, S., von Eynatten, H., Zack, T., 2012. A recipe for the use of rutile in sedimentary provenance analysis. Sediment. Geol. 282, 268–275. https://doi.org/10.1016/j.sedgeo.2012.09.008.

Valinasab Zarnagh, F., Moayyed, M., Jahangiri, A., Azizi, H., 2022. Mineral chemistry, thermobarometry and genesis of clinopyroxenes in Silurian mafic metavolcanic rocks of Maku, North West of Iran. Sci. q. J. Geosci. 32 (4), 15–28. https://doi.org/10.22071/gsj.2022.307112.1944.

Vecoli, M., Le Hérissé, A., 2004. Biostratigraphy, taxonomic diversity and patterns of morphological evolution of Ordovician acritarchs (organic-walled microphytoplankton) from the northern Gondwana margin in relation to palaeoclimatic and palaeogeographic changes. Earth-Sci. Rev. 67 (3), 267–311. https://doi.org/10.1016/j.earscirev.2004.03.002.

Vennin, E., Kolodka, C., Asghari, A., Thomazo, C., Buoncristiani, J.F., Goodarzi, H., Desaubliaux, G., 2015. Discussion on Palaeozoic discontinuities in the Kuh-e Surmeh area (Zagros, Iran). Mar. Pet. Geol. 66, 1073–1092. https://doi.org/10.1016/j.marpetgeo.2015.05.019.

Vermeesch, P., 2018. IsoplotR: A free and open toolbox for geochronology. Geosci. Front. 9 (5), 1479–1493. https://doi.org/10.1016/j.gsf.2018.04.001.

Vervoort, J.D., Blichert-Toft, J., 1999. Evolution of the depleted mantle: Hf isotope evidence from juvenile rocks through time. Geochim. Cosmochim. Acta 63 (3), 533–556. https://doi.org/10.1016/S0016-7037(98)00274-9.

Vesali, Y., Esmaeily, D., Moazzen, M., Chiaradia, M., Morishita, T., Soda, Y., Sheibi, M., 2020. The paleozoic Jalal Abad mafic complex (Central Iran): Implication for the petrogenesis. Geochemistry 80, (1). https://doi.org/10.1016/j.chemer.2020.125597 125597.

Wang, W., Cawood, P.A., Pandit, M.K., Xia, X., Raveggi, M., Zhao, J., Zheng, J., Qi, L., 2020. Fragmentation of South China from greater India during the Rodinia-Gondwana transition. Geology 49 (2), 228–232. https://doi.org/10.1130/G48308.1.

Wei, B., Cheng, X., Domeier, M., Jiang, N., Wu, Y., Zhang, W., Wu, K., Wang, B., Xu, P., Xing, L., Zhang, D., Li, T., Deng, X., Liu, F., Zhou, Y., Wu, H., 2022. Placing Another Piece of the Tethyan Puzzle: The First Paleozoic Paleomagnetic Data From the South Qiangtang Block and Its Paleogeographic Implications. Tectonics 41 (10). https://doi.org/10.1029/2022TC007355.

Wensink, H., 1983. Paleomagnetism of red beds of Early Devonian age from Central Iran. Earth Planet. Sci. Lett. 63 (2), 325–334. https://doi.org/10.1016/0012-821X(83)90045-6.

Whitehouse, M.J., Windley, B.F., Ba-Bttat, M.A.O., Fanning, C.M., Rex, D.C., 1998. Crustal evolution and terrane correlation in the eastern Arabian Shield, Yemen: geochronological constraints. J. Geol. Soc. 155 (2), 281–295. https://doi.org/10.1144/gsjgs.155.2.0281.

Whitehouse, M.J., Stoeser, D.B., Stacey, J.S., 2001. The Khida Terrane — Geochronological and Isotopic Evidence for Paleoproterozoic and Archean Crust in the Eastern Arabian Shield of Saudi Arabia. Gondwana Res. 4 (2), 200–202. https://doi.org/10.1016/S1342-937X(05)70695-X.

Whitehouse, M.J., Pease, V., Al-Khirbash, S., 2016. Neoproterozoic crustal growth at the margin of the East Gondwana continent – age and isotopic constraints from the easternmost inliers of Oman. Int. Geol. Rev. 58 (16), 2046–2064. https://doi.org/10.1080/00206814.2016.1207207.

Wilde, S., Youssef, K., 2002. A re-evaluation of the origin and setting of the Late Precambrian Hammamat Group based on SHRIMP U-Pb dating of detrital zircons from Gebel Umm Tawat, North Eastern Desert. Egypt. *J. Geol. Soc.* 159 (5), 595. https://doi.org/10.1144/0016-764901-081.

Wilmsen, M., Fürsich, F.T., Seyed-Emami, K., Majidifard, M.R., Taheri, J., 2009. The Cimmerian Orogeny in northern Iran: tectono-stratigraphic evidence from the foreland. Terra Nova 21 (3), 211–218. https://doi.org/10.1111/j.1365-3121.2009.00876.x.

Windley, B.F., Whitehouse, M.J., Ba-Bttat, M.A.O., 1996. Early Precambrian gneiss terranes and Pan-African island arcs in Yemen: Crustal accretion of the eastern Arabian Shield. Geology 24 (2), 131–134. https://doi.org/10.1130/0091-7613(1996)024<0131:EPGTAP>2.3.CO;2.

Wu, L., Murphy, J.B., Quesada, C., Li, Z.-X., Waldron, J.W.F., Williams, S., Pisarevsky, S., Collins, W.J., 2020. The amalgamation of Pangea: Paleomagnetic and geological observations revisited. Geol. Soc. Am. Bull. 133 (3–4), 625–646. https://doi.org/10.1130/B35633.1.

Yeshanew, F.G., Pease, V., Whitehouse, M.J., Al-Khirbash, S., 2015. Zircon U-Pb geochronology and Nd isotope systematics of the Abas terrane, Yemen: Implications for Neoproterozoic crust reworking events. Precambrian Res. 267, 106–120. https://doi.org/10.1016/j.precamres.2015.05.037.

Yeshanew, F.G., Pease, V., Abdelsalam, M.G., Whitehouse, M.J., 2017. Zircon U-Pb ages, δ18O and whole-rock Nd isotopic compositions of the Dire Dawa Precambrian basement, eastern Ethiopia: implications for the assembly of Gondwana. J. Geol. Soc. 174 (1), 142–156. https://doi.org/10.1144/jgs2016-017.

Zack, T., Kooijman, E., 2017. Petrology and Geochronology of Rutile. Rev. Mineral. Geochem. 83 (1), 443–467. https://doi.org/10.2138/rmg.2017.83.14.

Zanchetta, S., Berra, F., Zanchi, A., Bergomi, M., Caridroit, M., Nicora, A., Heidarzadeh, G., 2013. The record of the Late Palaeozoic active margin of the Palaeotethys in NE Iran: Constraints on the Cimmerian orogeny. Gondwana Res. 24 (3), 1237–1266. https://doi.org/10.1016/j.gr.2013.02.013.

Zanchi, A., Zanchetta, S., Berra, F., Mattei, M., Garzanti, E., Molyneux, S., Nawab, A., & Sabouri, J. (2009a). The Eo-Cimmerian (Late? Triassic) orogeny in North Iran. In M. F. Brunet, M. Wilmsen, & J. W. Granath (Eds.), *South Caspian to Central Iran Basins* (Vol. 312, pp. 0). Retrieved from https://doi.org/10.1144/SP312.3 doi:10.1144/SP312.3.

Zanchi, A., Zanchetta, S., Garzanti, E., Balini, M., Berra, F., Mattei, M., Muttoni, G., 2009b. The Cimmerian evolution of the Nakhlak-Anarak area, Central Iran, and its bearing for the reconstruction of the history of the Eurasian margin. Geol. Soc. Spec. Pub. 312 (1), 261–286. https://doi.org/10.1144/SP312.13.

Zanchi, A., Malaspina, N., Zanchetta, S., Berra, F., Benciolini, L., Bergomi, M., Cavallo, A., Javadi, H.R., Kouhpeyma, M., 2015. The Cimmerian accretionary wedge of Anarak Central Iran. J. Asian Earth Sci. 102, 45–72. https://doi.org/10.1016/j.jseaes.2014.08.030.

Zanchi, A., Zanchetta, S., Balini, M., Ghassemi, M.R., 2016. Oblique convergence during the Cimmerian collision: Evidence from the Triassic Aghdarband Basin NE Iran. *Gondwana Res.* 38, 149–170. https://doi.org/10.1016/j.gr.2015.11.008.

Zoheir, B., Zeh, A., El-Bialy, M., Ragab, A., Deshesh, F., Steele-MacInnis, M., 2021. Hybrid granite magmatism during orogenic collapse in the Eastern Desert of Egypt: Inferences from whole-rock geochemistry and zircon U-Pb–Hf isotopes. Precambr. Res. 354,. https://doi.org/10.1016/j.precamres.2020.106044 106044.

Zoleikhaei, Y., Mulder, J.A., Cawood, P.A., 2021. Integrated detrital rutile and zircon provenance reveals multiple sources for Cambrian sandstones in North Gondwana. Earth-Sci. Rev. 213,. https://doi.org/10.1016/j.earscirev.2020.103462 103462.

Zoleikhaei, Y., Mulder, J.A., Cawood, P.A., 2022. Evaluating sediment recycling through combining inherited petrogenic and acquired sedimentary features of multiple detrital minerals. Basin Res. 34 (3), 1055–1083. https://doi.org/10.1111/bre.12650.